

## CEDAR Tutorial #3

Thursday June 28, 2007

### State of the art in mesosphere science

John Meriwether

Department of Physics and Astronomy

Clemson University

- 22+ years of progress since “ignorasphere” was coined to describe our understanding of the mesosphere region.
- Too many slides! (solution: leave major portion for supplements)
- Talk primarily focused upon lidar results because mesospheric dynamics is the major focus of the talk. There is no substitute for vertical profiles of U, V, and T

## Outline:

- Introduction: basic information regarding mesosphere
- Instrumental techniques for mesosphere observations (briefly)
- Mesosphere aeronomy science
  - ✓ Mesosphere inversion layer(s)
  - ✓ Mesosphere dynamics re instabilities
- Closing comments

Talk not really state-of-the-art but more a review, a refresher, with emphasis upon mesosphere dynamics based upon recent publications

Three talks this week in GW workshop by Fritts, Swenson, and Walterscheid of great interest and cutting edge science

## What is so interesting about the mesosphere?

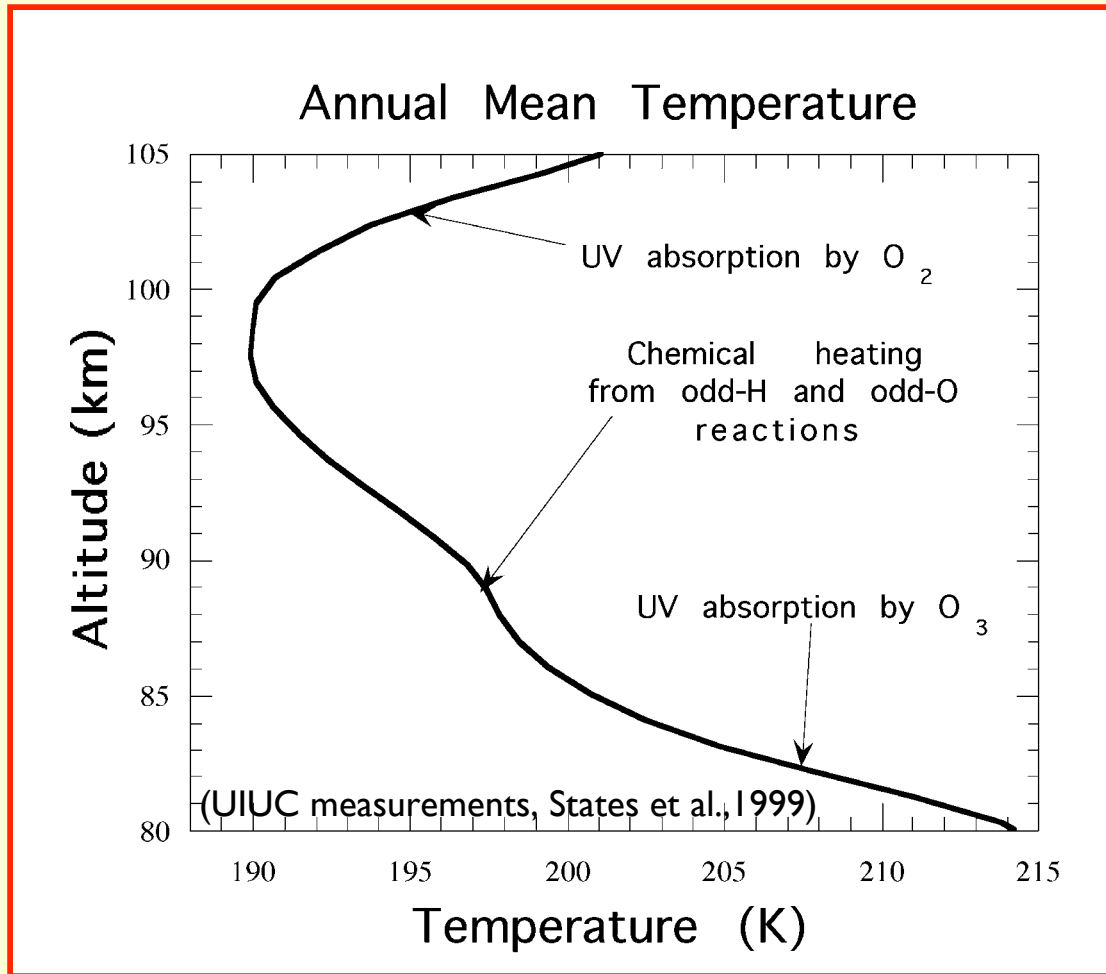
- Narrow slice of atmosphere - 20-30 km thickness with marginal dynamical stability
- Marks end of fully mixed atmosphere called “homosphere”
- Highly dynamic region (where waves break and turbulence structures are created)
- Complex region featuring transition from hydrodynamic flow to molecular diffusion
- Observation very contrary to physical intuition:
  - lowest temperatures on Earth in summer polar region; PMCs
  - warm in winter polar night where there is no solar irradiation - where does this energy come from?
- Location of entry region of meteoric debris
- Exotic chemistry, several airglow layers (OH, O<sub>2</sub>, and O), mesospheric bores, QP echoes, sporadic layers

# Observing Techniques

(see supplement for details)

- In-situ
    - Rockets
  - Ground-based
    - Radar (ISR, MF, meteor)
    - Lidar - Rayleigh, resonance ( Na, K, Fe)
    - Passive optics -imager(OH, O, O<sub>2</sub>), FPI (T), spectrograph (T)
  - Satellite
    - Limb scanning
    - nadir
- List not exhaustive

# Averaged Thermal Structure of Mesopause Region



Schuman-Runge Bands  
& Continuum 135-200 nm

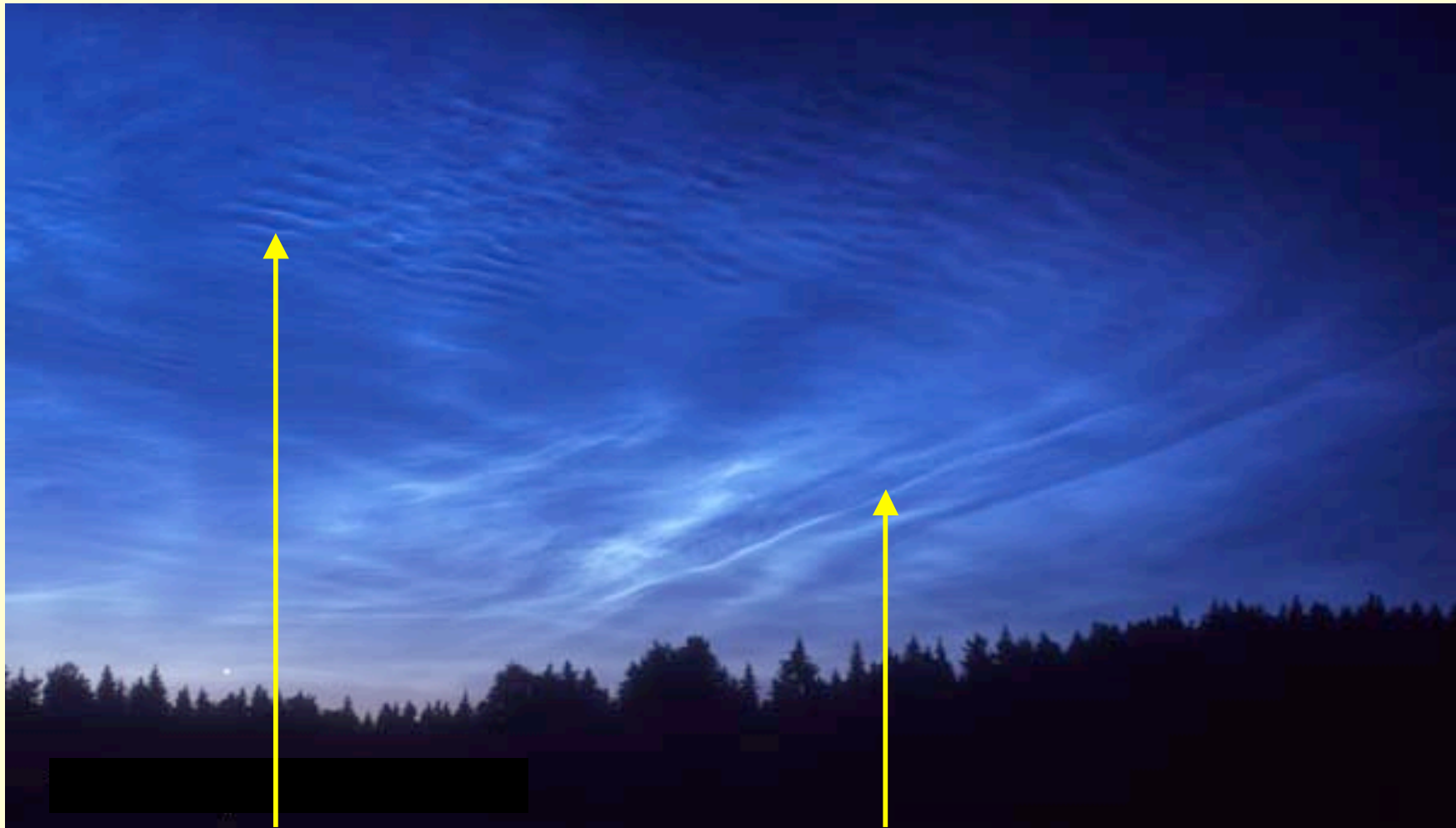
Lyman- $\alpha$  line 121.5 nm

Hartley Band  
200-300 nm

IR Radiative Cooling  
By CO<sub>2</sub> (15 $\mu$ m)

Illinois lidar observations show chemical heating as relatively weak source:  
from States et al.[1999]

## PMCs display complicated structure caused by GW activity



**Billows**

**Bands**

Timo Leponiemi, 2001

Dynamics of mesosphere highly influenced by GWs and tidal waves

## Multiple GW Sources

- Flow over a mountain range
- Flow over convective cloud (moving mountain)
- Kelvin-Helmholtz instability around the jet stream
- Geostrophic adjustment

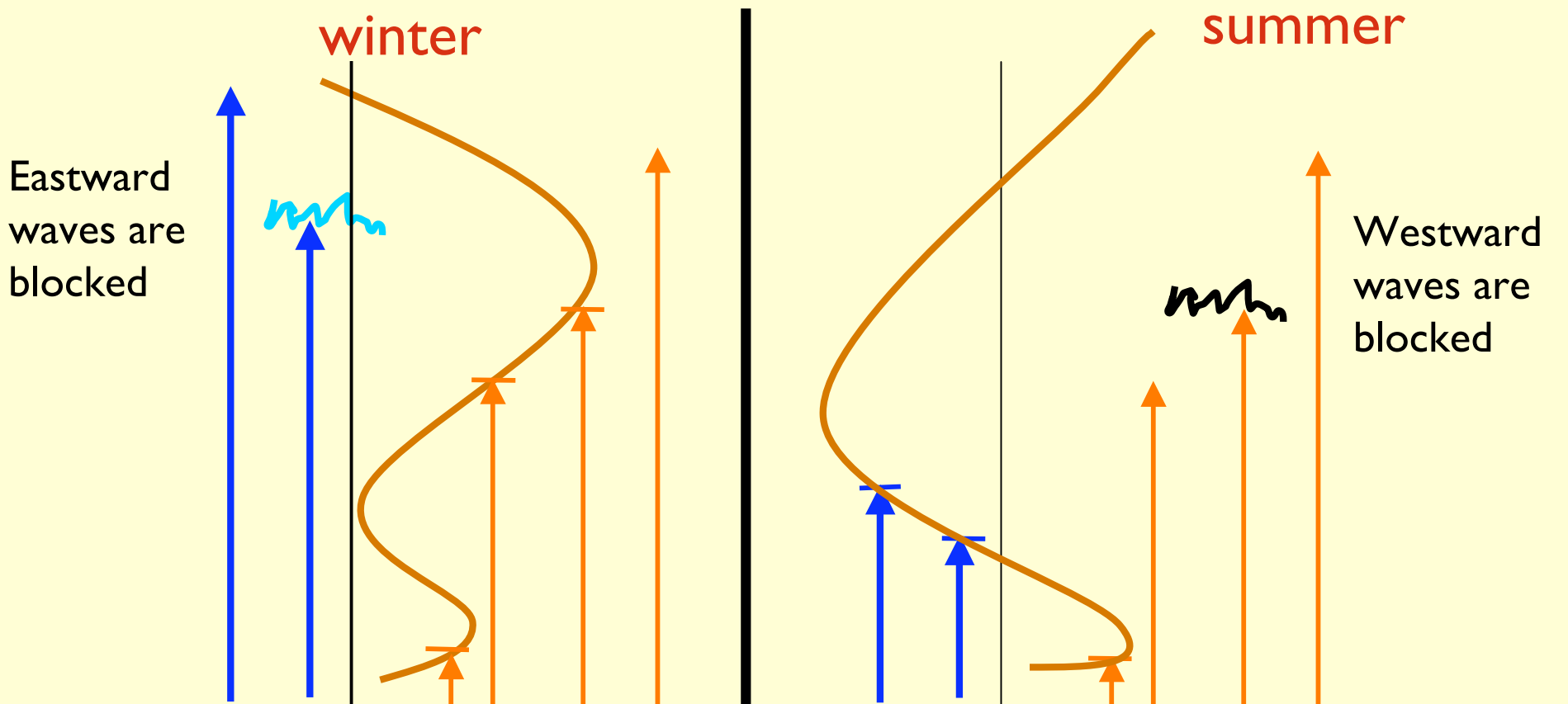


Collection of slides in supplemental material concerning properties of GWs re behavior and math. theory

## Change of Gravity Wave Forcing between summer and winter

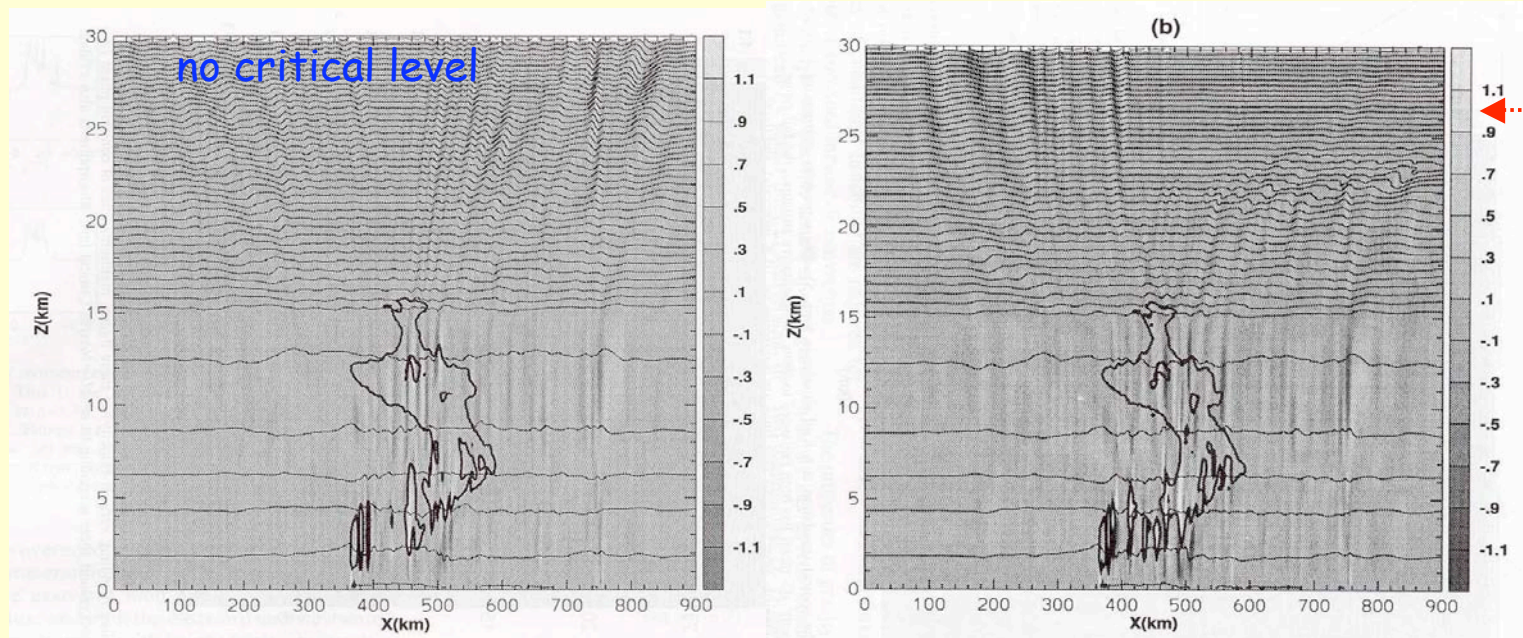
Filtering of gravity waves by stratospheric wind system: gravity wave will be reflected or absorbed at critical layer.

- Eastward stratospheric jet under normal winter conditions: dominant westward propagating gravity waves in the mesosphere.
- Stratospheric wind reversal during equinox: dominant direction of gravity wave in mesosphere also reverses due to filtering.





## Model simulation of gravity waves forced by deep convection

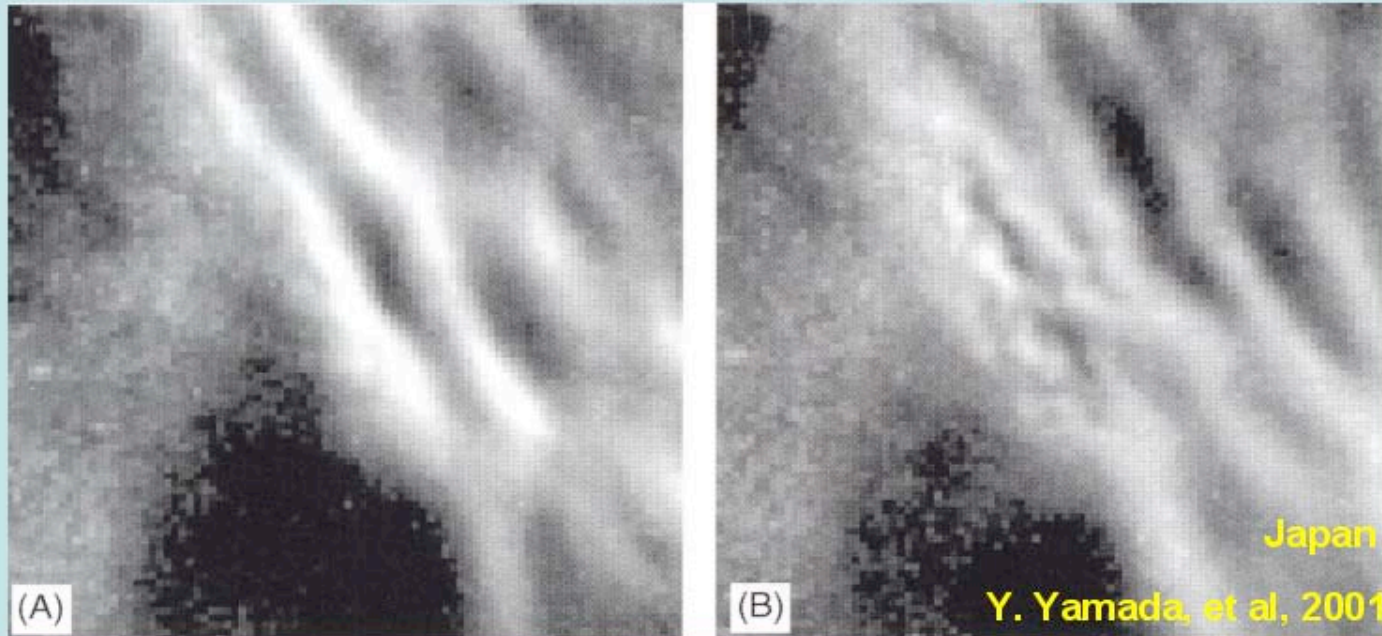


Alexander and Holton, 2000

Convective activity (e.g., thunderstorms) generate GW wave packet events in copious quantities but many of these are blocked by critical layer filtering in stratosphere

What does a breaking GW event look like?

## Example of Wave Breaking Event



- Short-period gravity waves break at mesospheric altitudes, depositing large amounts of momentum.
- Gravity wave events are episodic yet their effects are global.
- Source anisotropy and wave propagation remain major unknowns.

Courtesy, M. Taylor

Taylor et al., 1994

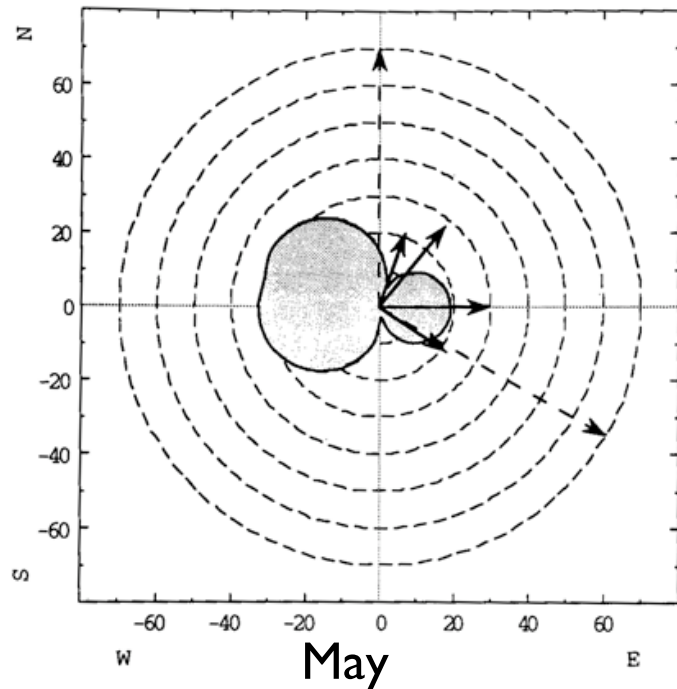


Fig. 5. Blocking diagram for May at 85 km. The shaded area indicates the magnitude and direction of the restricted region for wave propagation to OH heights. The solid arrows show the magnitude and direction of the wave motions observed during this month, while the dashed arrows indicate direction only.

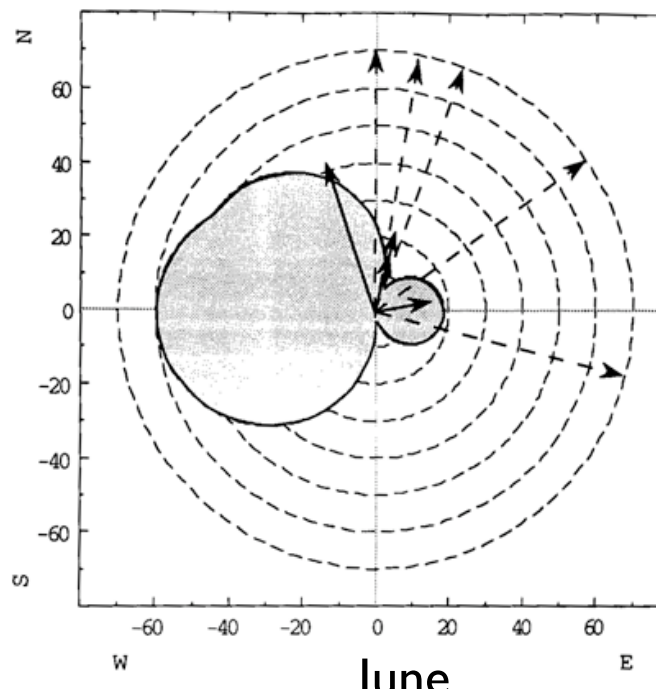
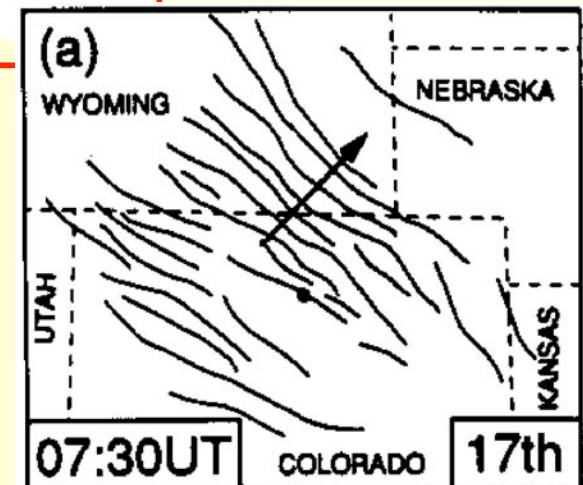


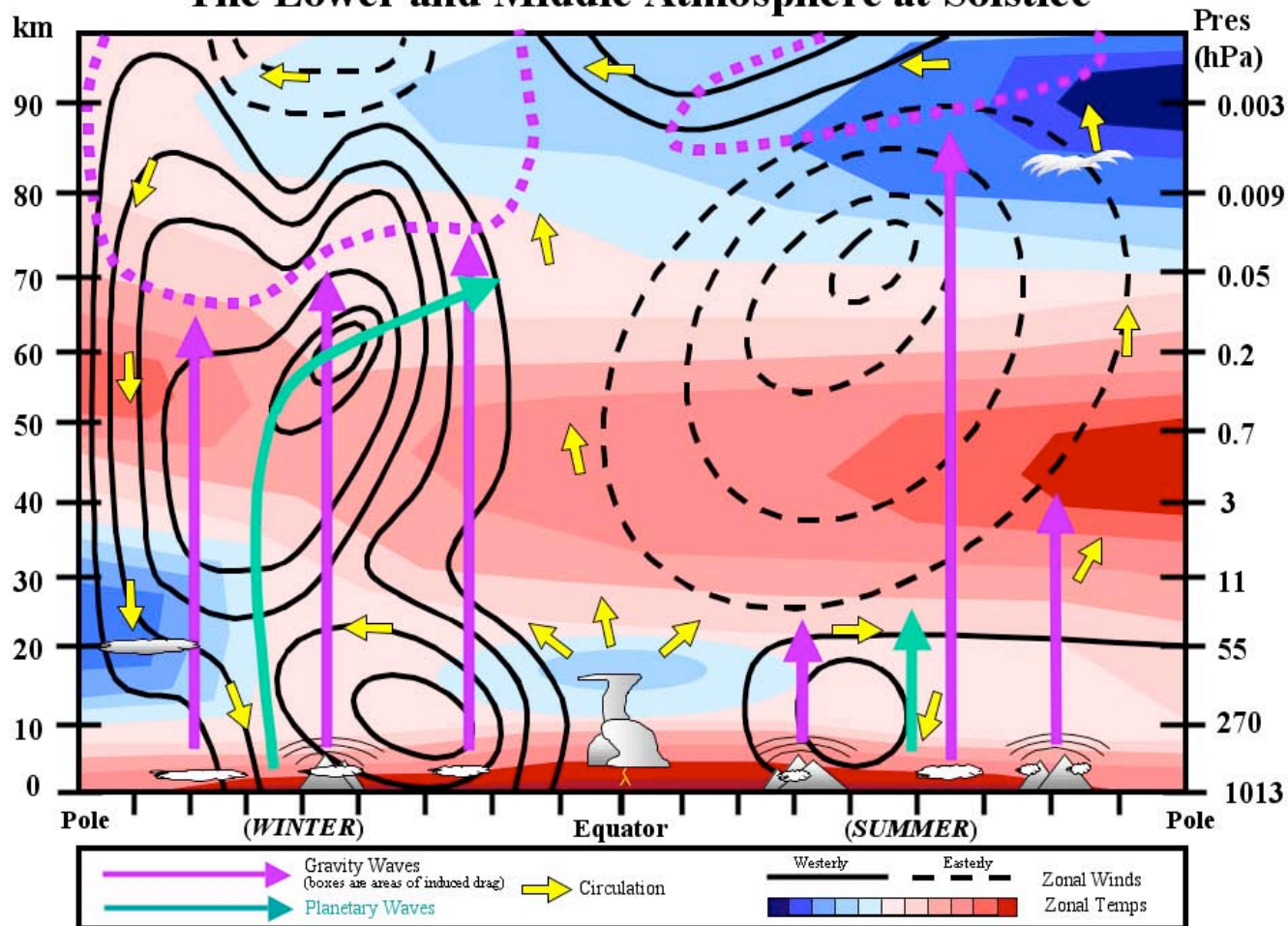
Fig. 6. Blocking diagram for June at 85 km. For comparison the results are plotted on the same scale as Figure 5. Frequent changes in the observing conditions during this month limited the velocity measurements of several displays to direction only.

Blocking diagrams represent wave propagation azimuths that are filtered by tropospheric and stratospheric winds. Result is dominance by poleward propagating waves.

ASC imaging observations for OH indicate preferential propagation directions for GW events seen



## The Lower and Middle Atmosphere at Solstice

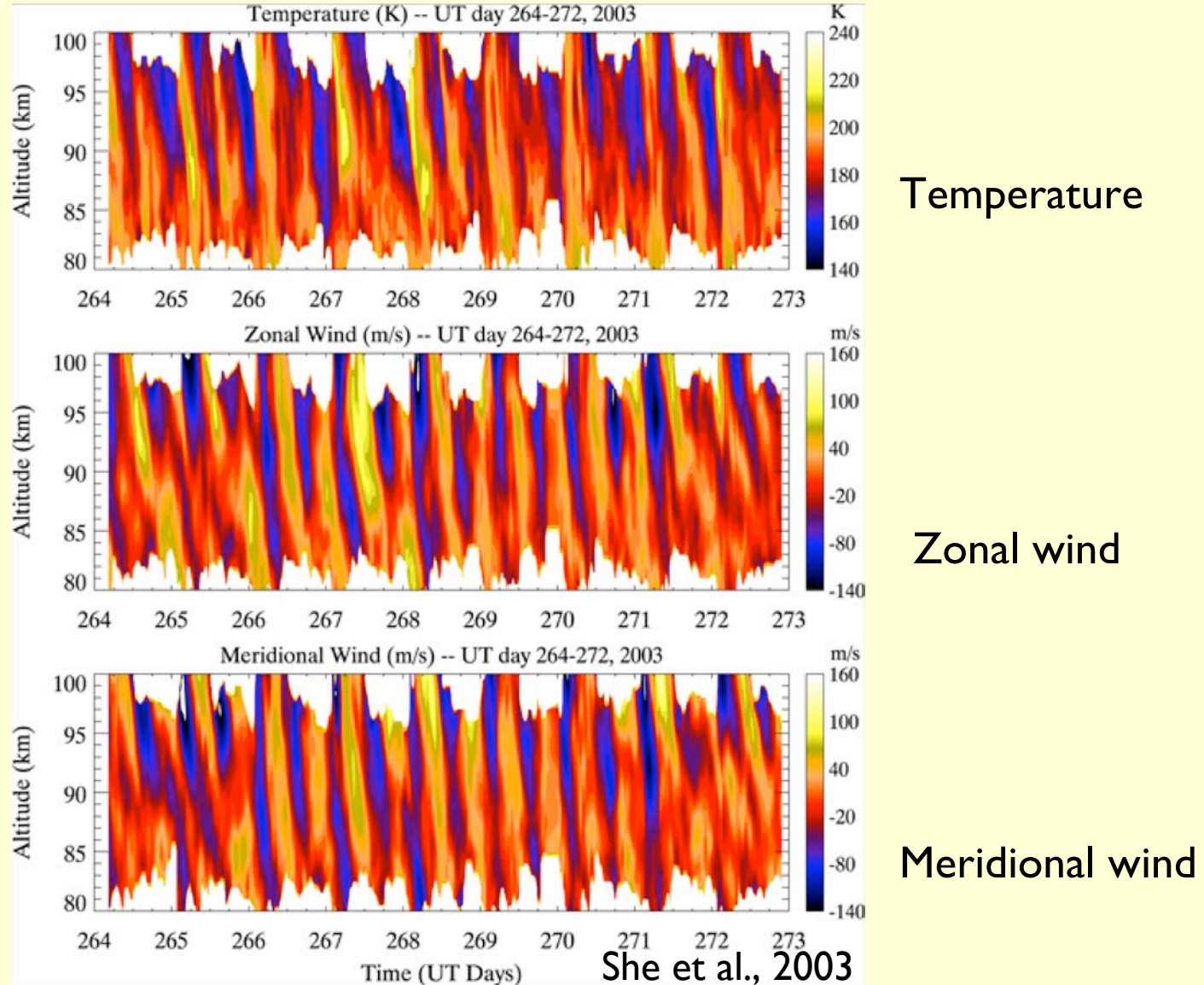


Mesosphere exhibits complex circulation indicating region is far from radiative equilibrium: **cold in the summer, warm in the winter**

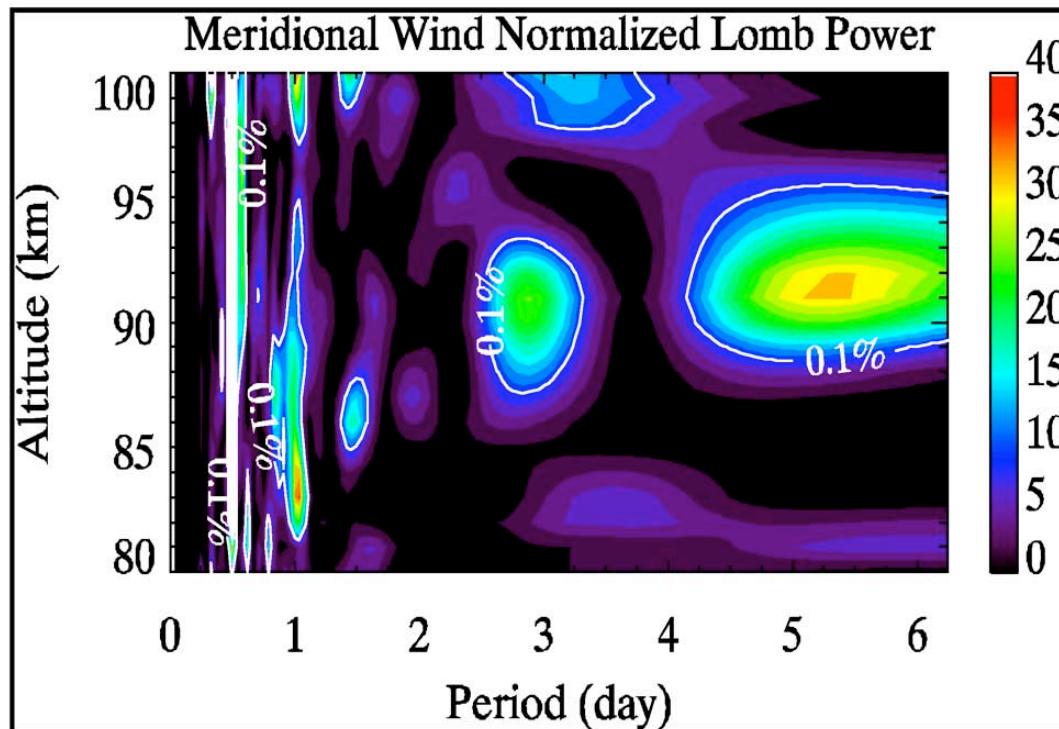
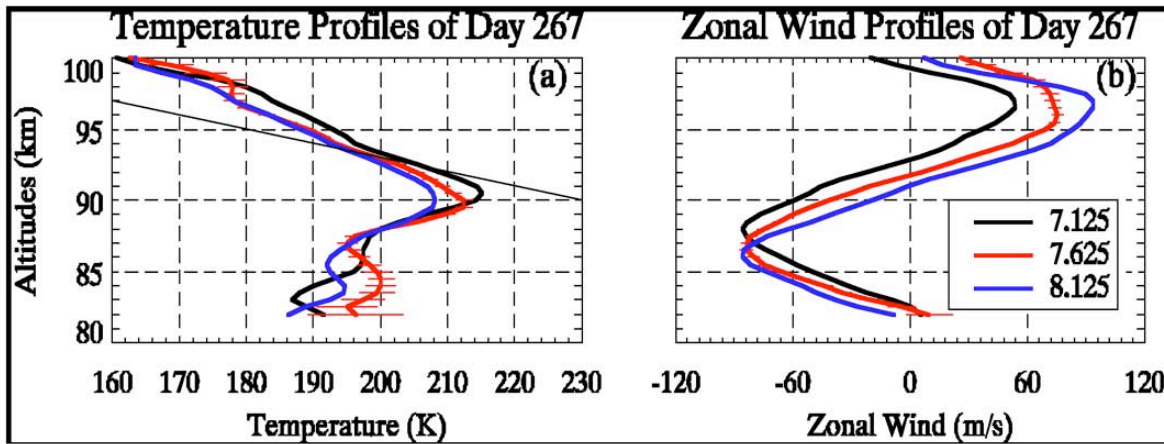
Winter GW breaking induces reversal of mesospheric zonal jet and generates residual meridional circulation pattern featuring rising air in summer and sinking air in winter

Tidal waves (diurnal, semi-diurnal, terdiurnal) are also important players in MLT dynamics.

## Tidal waves play major role in mesospheric dynamics



Results obtained for a 9 day continual run by the CSU UVT lidar illustrate the variability of the tidal structure in response to GW and tidal fluctuations.



Note the high winds seen in the 95-100 km region.

Top side of the T profiles is nearly adiabatic indicating marginal stability.

Schmidlin and colleagues detected Mesosphere Inversion Layers in rocket measurements of mesospheric thermal profile in 1976 at Wallop Island

Rayleigh lidar system did not exist at the time to explore these early results.



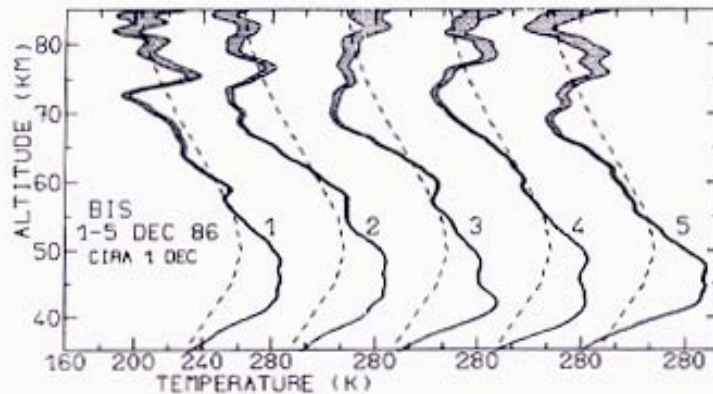


Fig. 1 Nightly mean temperature profiles at Biscarrosse from December 1 to December 5, 1986. The error bars ( $\pm 1\sigma$ ) are indicated by the shaded area. The CIRA 1972 profile is shown for comparison (dotted line). Perturbations with vertical wavelengths shorter than 1.5 km have been filtered.

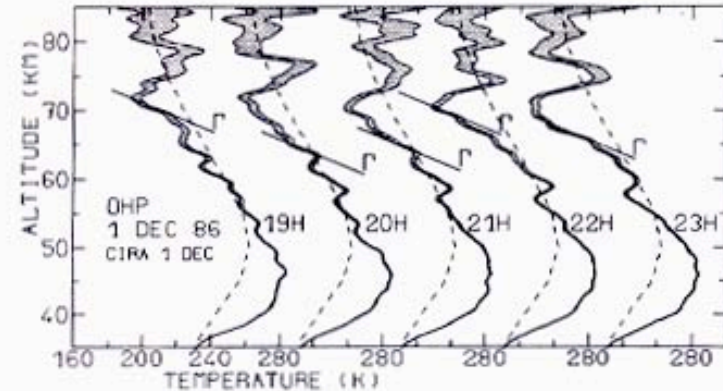


Fig. 3 Hourly mean temperature profiles on December 1, 1986 at OHP. The adiabatic lapse rate  $\Gamma$  is represented for comparison in the layer of strong negative lapse rates.

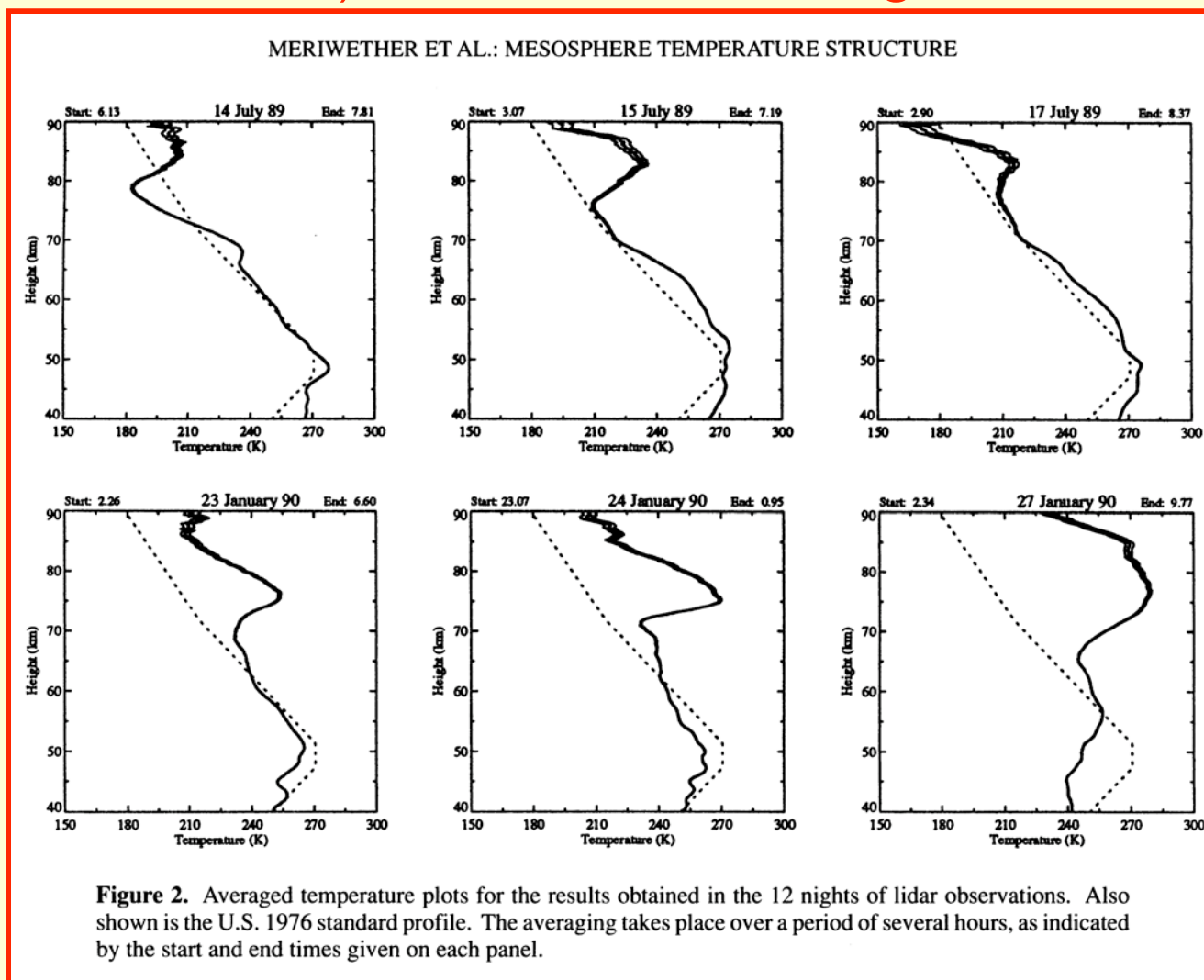
Hauchecorne et al., 1987

Nightly means, successive winter nights

Hourly progression

Rayleigh lidar results from Chanin and her colleagues: First results via ground-based soundings.

## WP Rayleigh observations illustrate upper MILs (during summer) and lower MILs during winter



Meriwether et al., 1994

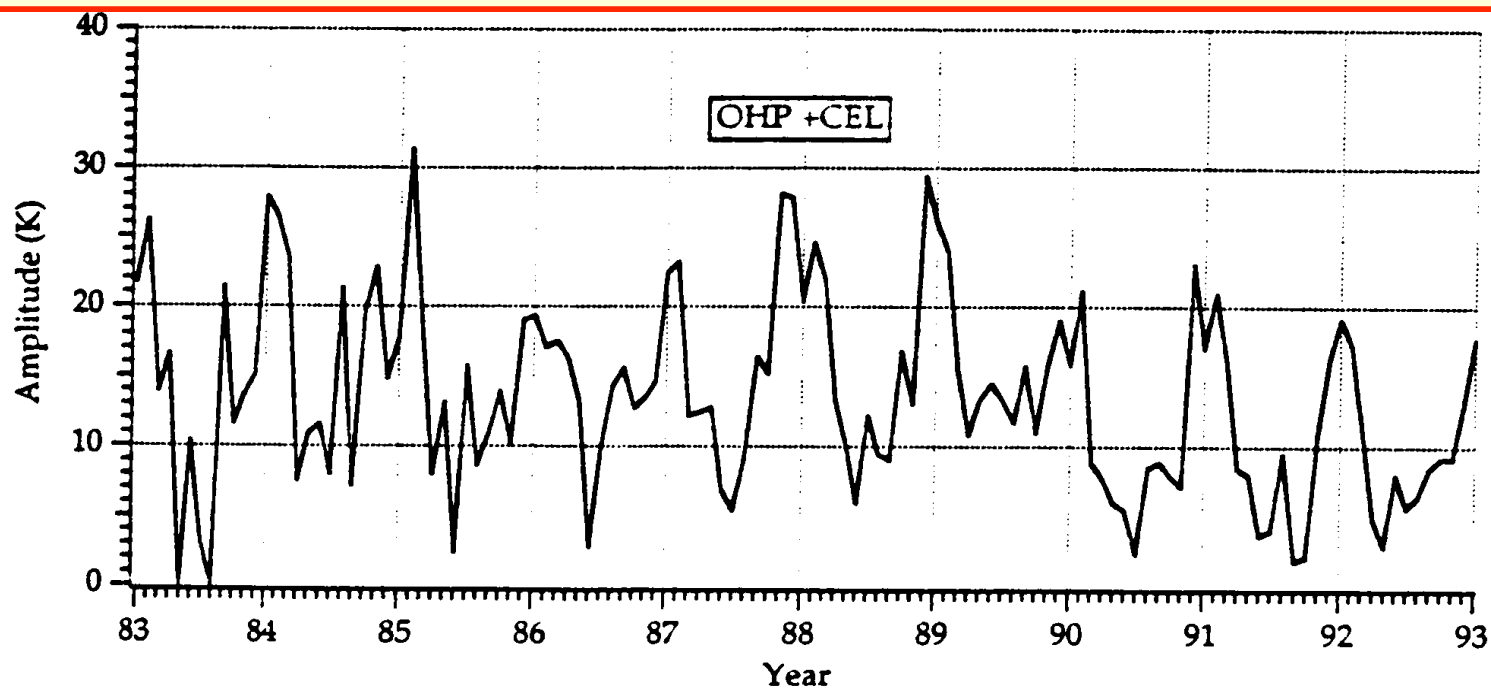
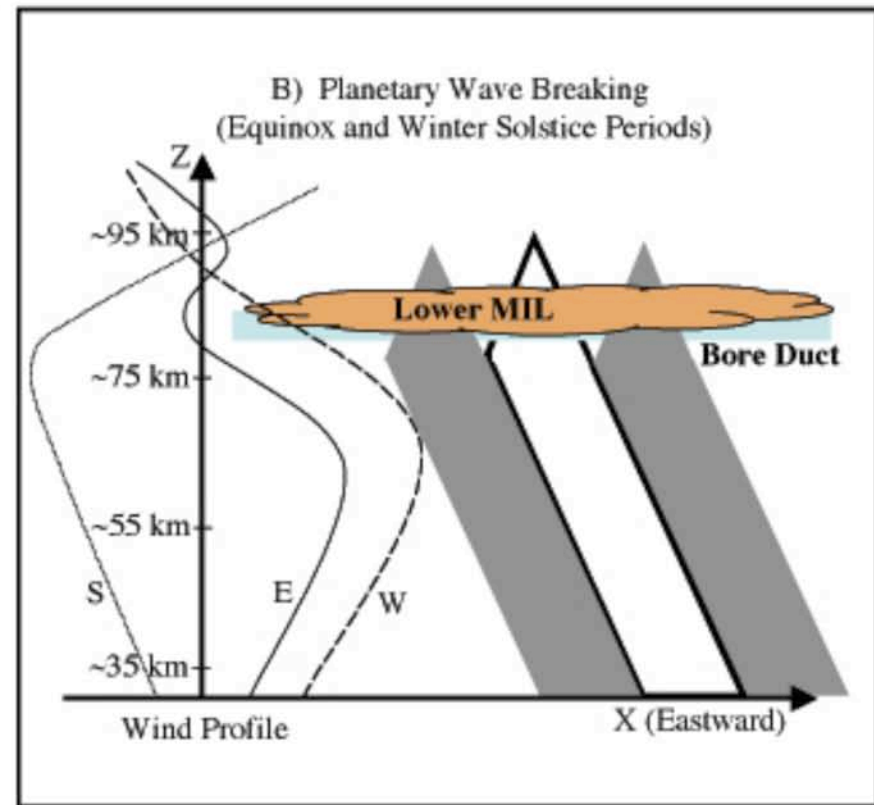
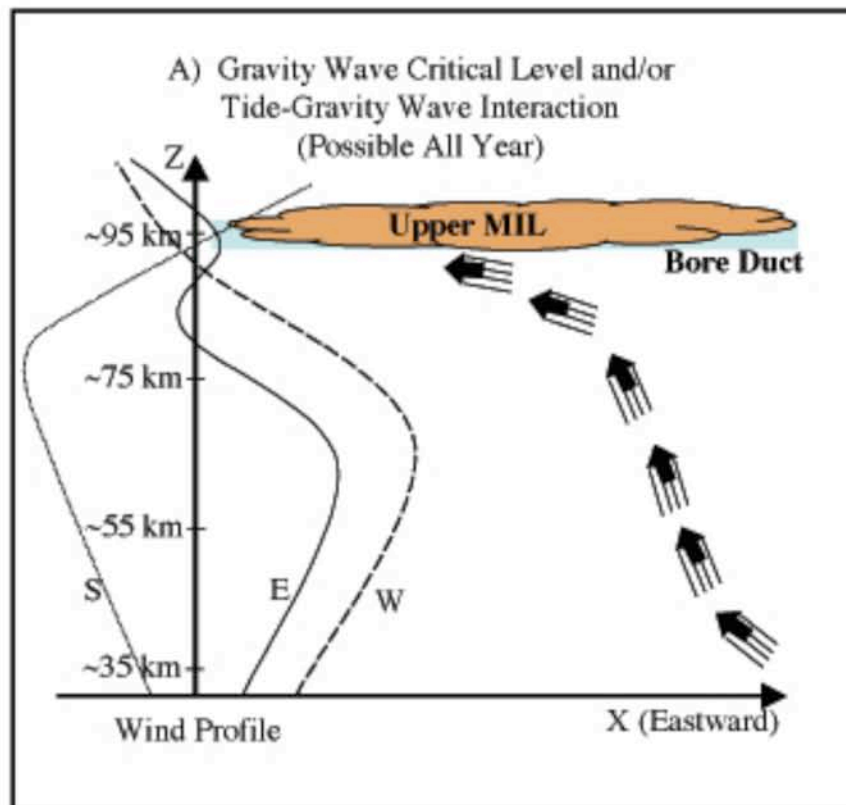


**Figure 3.** Monthly mean amplitude of temperature inversions seen by Rayleigh lidar at OHP and CEL.

From LeBlanc and Hauchecorne [J. Geophys. Res., 1999]

Variations in MIL amplitudes over ten year duration show minimum amplitudes for summers indicating forcing less vigorous in summer; also, occurrence rate reduced in summer

Meriwether and Gerrard [2003] suggested that there are two forms of MIL events:



Hence, the distinction of the “upper” MIL and the “lower” MIL.

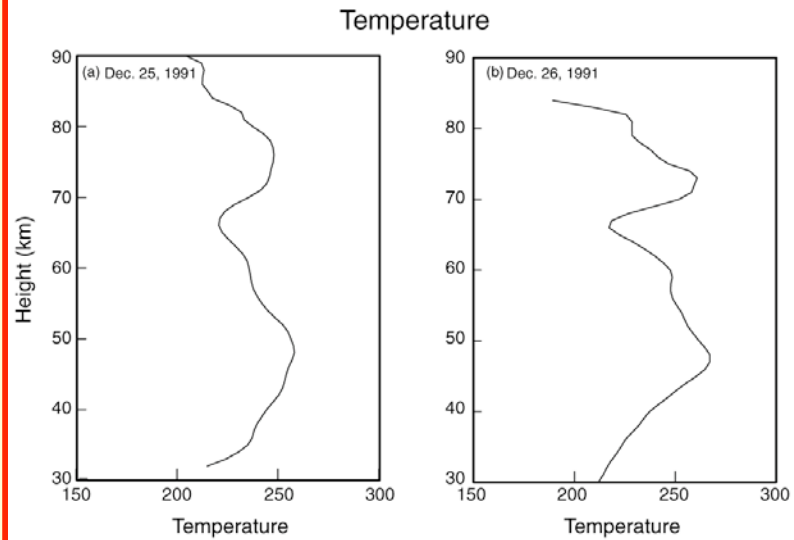


**Figure 1.** Temperature profile observed over OHP on (a) 25 December 1991 and (b) 26 December 1991.

French MIL observations

Salby et al.[2002] demonstrated using UARS data that planetary wave activity coincided with regional enhancement of T that overlaps with ground-based observations of MIL events.

Absorption of a planetary wave produces significant increase in T. Explanation applies only to “lower MILs” in winter.

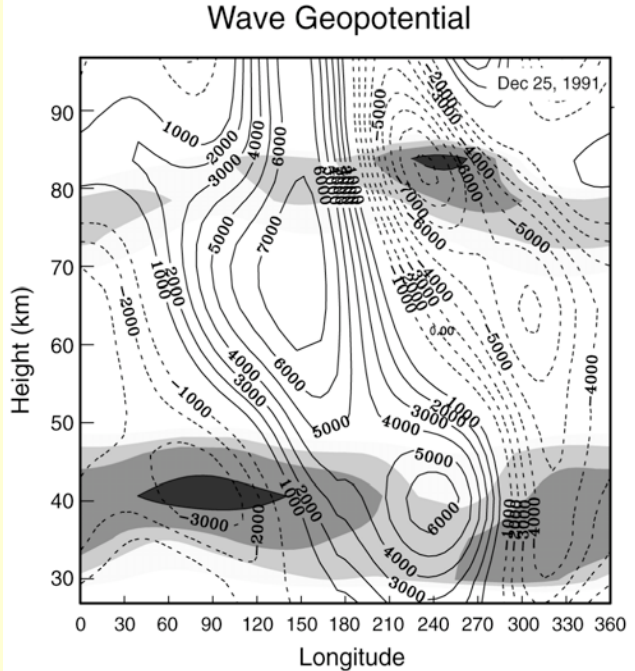
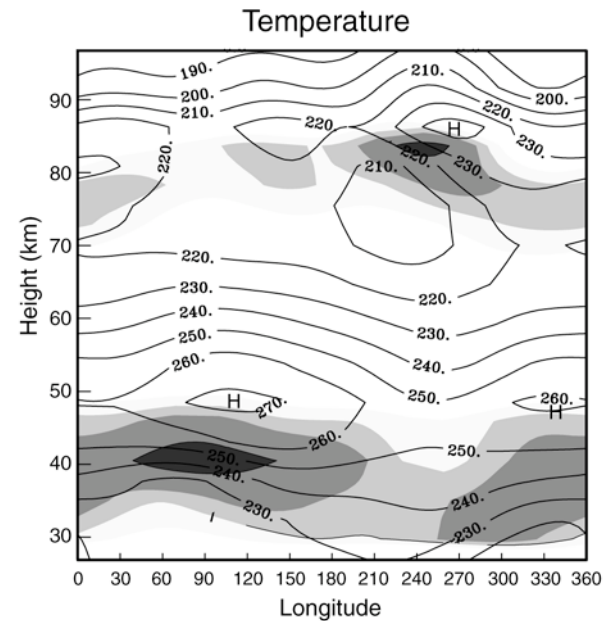
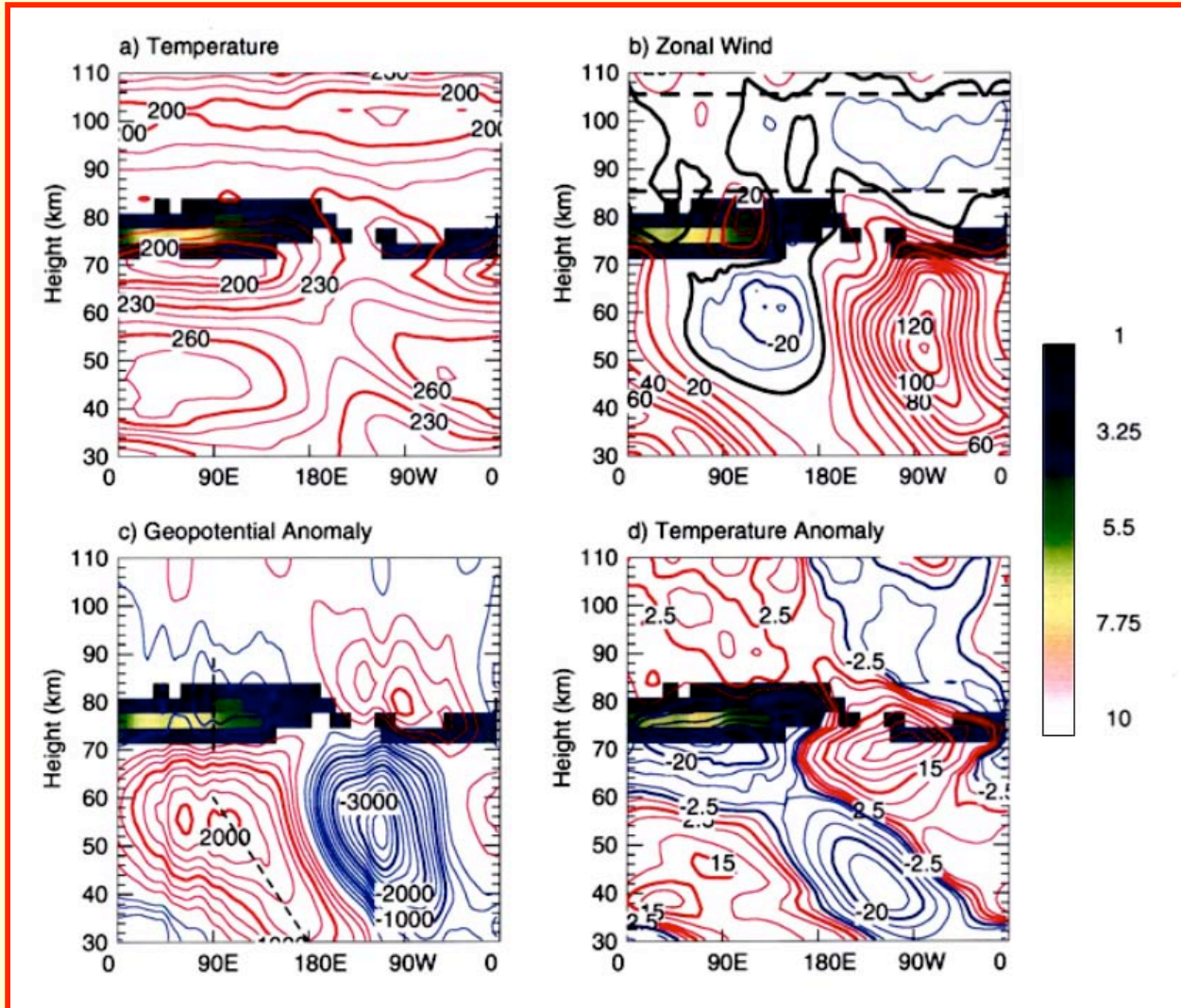


**Figure 6.** Wave geopotential ( $m^2 s^{-2}$ ) at  $44^\circ N$ , as a cross section of longitude and height, observed by UARS on 25 December 1991.

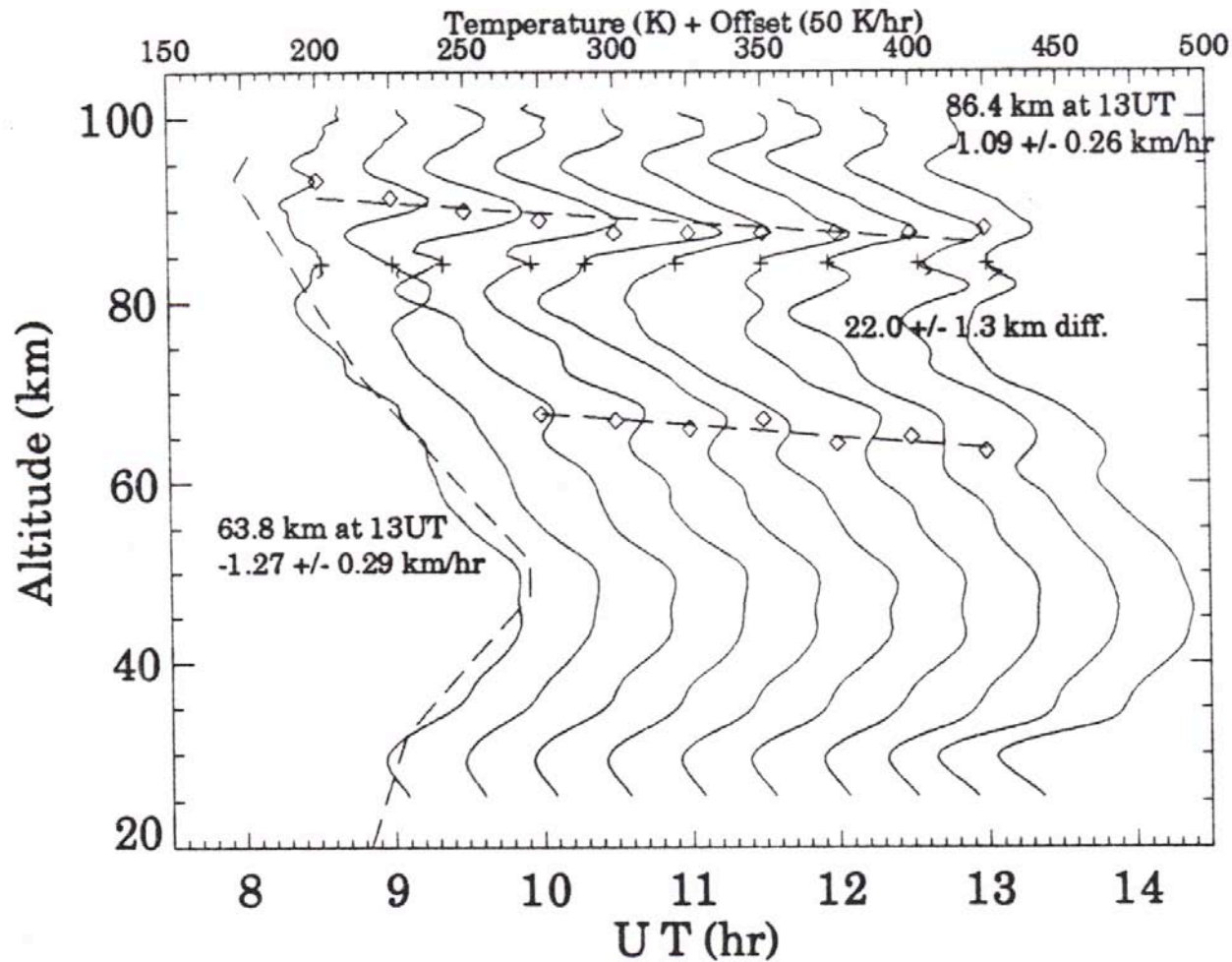
WACCM model calculations also show development of MIL events as a result of the absorption of PWs.



Black line in zonal wind plot represent locus of zero wind indicating that PW cannot propagate to higher altitudes.

The zero wind boundary is produced by breaking GW events that close the mesospheric wind jet.

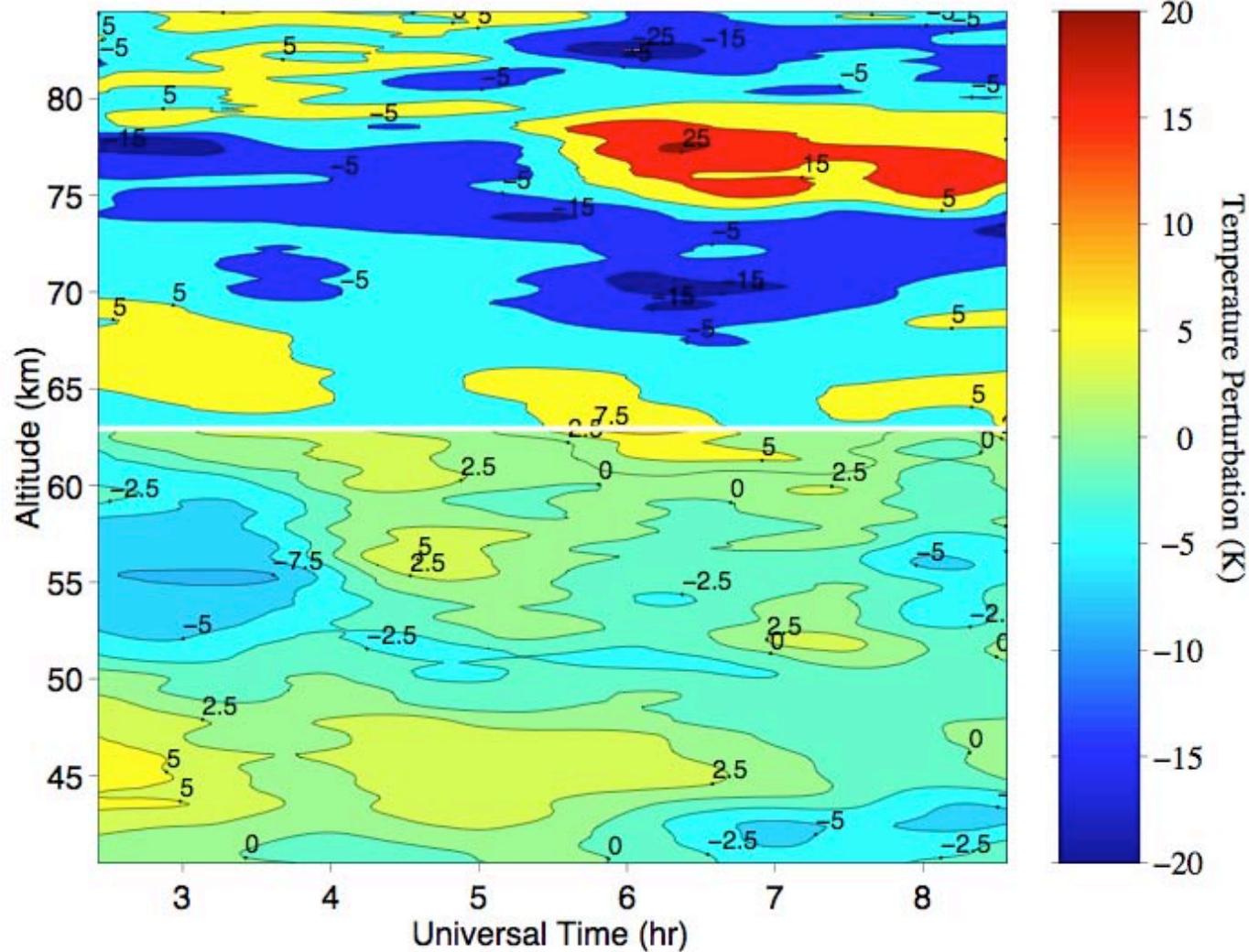
Sassi et al.,2003



Vertical separation that of the diurnal tide.

Combined ALOHA Rayleigh and Na temperature measurements show *TWO* MILs occurring simultaneously! (from Dao et al., 1993) suggesting tidal origin

Sica et al., 2003

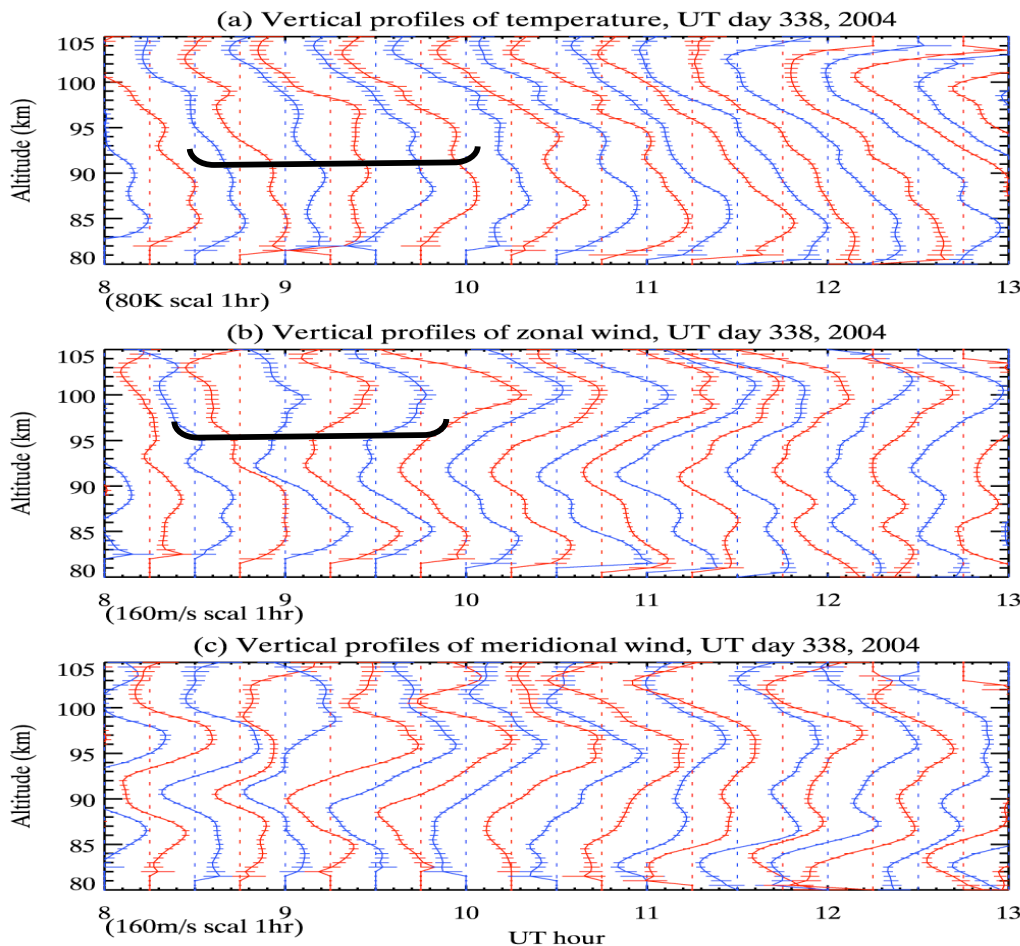


The turning of the diurnal tide releases GWs giving rise to a sudden increase in T at 77 km and a decrease in stability above the MIL event - further details in off-line version



What evidence do we have that GW breaking will increase  $T$  for the inversion layer peak and also increase the topside lapse rate, i.e., making the atmosphere become more unstable?

# CSU Na T, U, V lidar observes GW behavior at a critical layer.



T increases at 95 km

U increases at 98-100 km

Sudden increase in zonal wind is associated with the appearance of a GW event of horizontal wavelength 100 km, 1.8 hr period

**Figure 1.** Vertical profiles of (a) temperature, (b) zonal wind, and (c) meridional wind between 0800 and 1300 UT on the night of December 3rd (UT day 338), 2004. These profiles are spaced at 15 min intervals; whose horizontal scale also correspond to 20 K in temperature or 40 m/s in wind speed. The vertical dotted lines denote 200 K for temperature and 0 m/s for wind.

Li et al.,2007

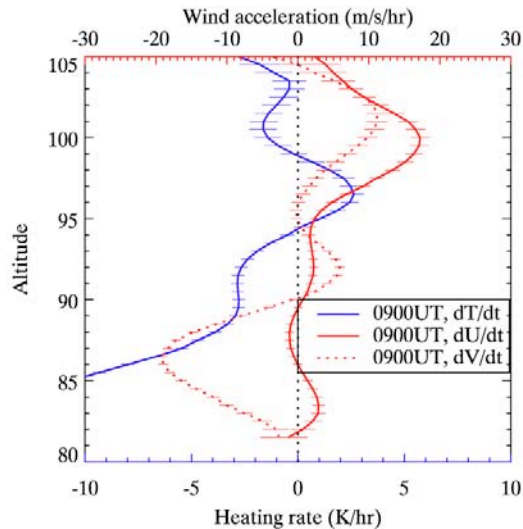


**Figure 3.** The heating rate, zonal wind acceleration, and meridional wind acceleration at 0900 UT on the night of December 3rd (UT day 338), 2004. The breaking region is near 100 km.

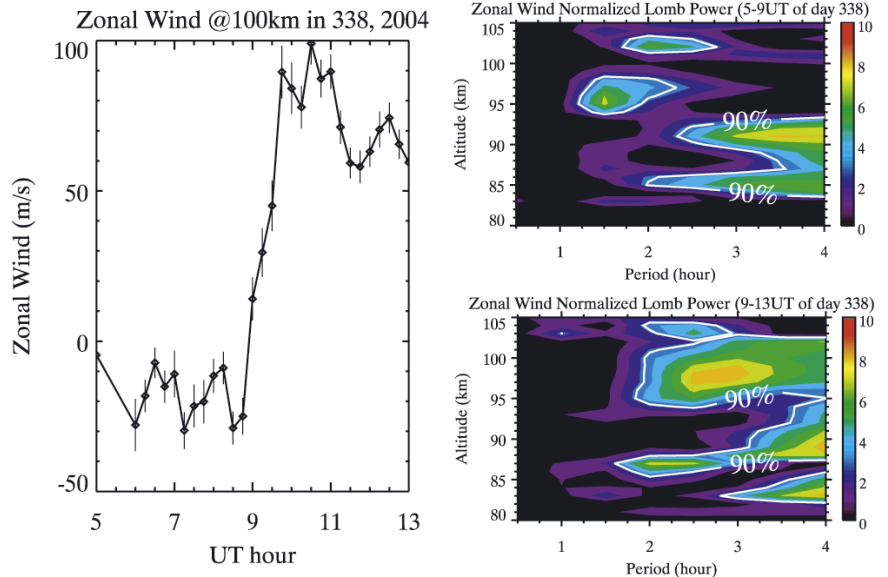


**Figure 2.** (left) The plot for zonal wind vs. UT hour at 100 km and the contour plots of Lomb power spectra (top right) between 0500 and 0900 UT and (bottom right) between 0900 and 1300 UT. The 90% significant level is also plotted with white lines in the Lomb power contours.

Cooling at 100 km, heating below at 97 km

Analysis shows zonal wind acceleration as the GW breaking wave event occurs between 95 and 100 km - GW period of 1.8 hr.

Huang et.al.[2002] also suggested CL interaction as explanation for MIL development. See MIL supplement for figure of U and T ALOHA data.

## Local mean state changes due to gravity wave breaking modulated by the diurnal tide

Han-Li Liu, Maura E. Hagan, and Raymond G. Roble

High Altitude Observatory, National Center for Atmospheric Research, Boulder, Colorado

**Abstract.** During gravity wave breaking, heating rates are determined by wave advection, turbulent diffusion, and turbulence dissipative heating. A series of numerical experiments show that the total heating rates can be large ( $\sim \pm 10 \text{ Kh}^{-1}$ ) and can cause large local temperature changes. The wave advection causes dynamical cooling in most of the wave breaking region, consistent with previous studies. Nonuniform vertical turbulent diffusion causes strong transient heating in the lower part of the wave breaking region and cooling above. The dissipative heating rate is relatively small compared with those due to the dynamical cooling and turbulent diffusion. In these numerical experiments, zonal wind and temperature perturbations of the diurnal tide and the zonal mean zonal wind and temperature compose the background state for the computation. This is used to examine the idea that temperature inversions, often observed in the mesosphere, are related to the gravity wave and tidal wave interactions. The simulation results show that the large temperature changes in this process can form temperature inversion layers that progress downward with a speed similar to that of a diurnal tide phase speed, which clearly suggests the tidal modulation of the gravity wave and mean flow interactions. Such a process is dependent on season and latitude, because the background state stability varies with season and latitude. The development of the temperature inversion is also affected by the gravity wave characteristics. It is also shown that the local mean wind, wind shear, and chemical species can undergo large changes accompanying the temperature inversion.

Modelling work provides support for the idea that production of MIL occurs through a breaking GW event interacting with the background diurnal tidal wave

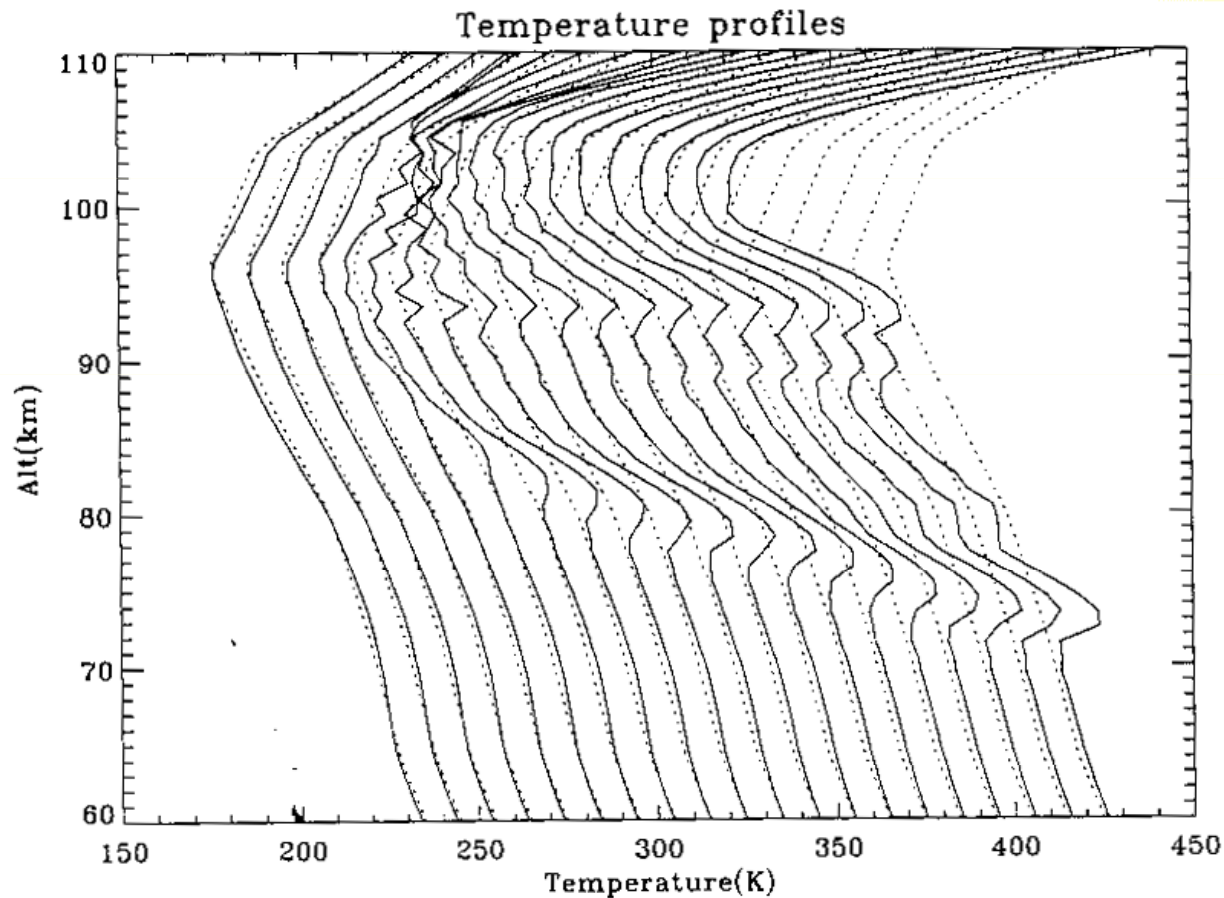


**Figure 5.** Temperature profiles from 1230 to 2200 LT with half-hour time intervals for J39. Each profile is shifted to the right by 10 K. The solid curves are profiles including zonal mean temperature, tidal perturbation, and local mean changes due to gravity wave breaking. The dotted curves are the zonal mean temperature profiles.

Calculations demonstrate that MILs can be produced due to the GW interacting with the diurnal tide decreasing stability and producing turbulence.

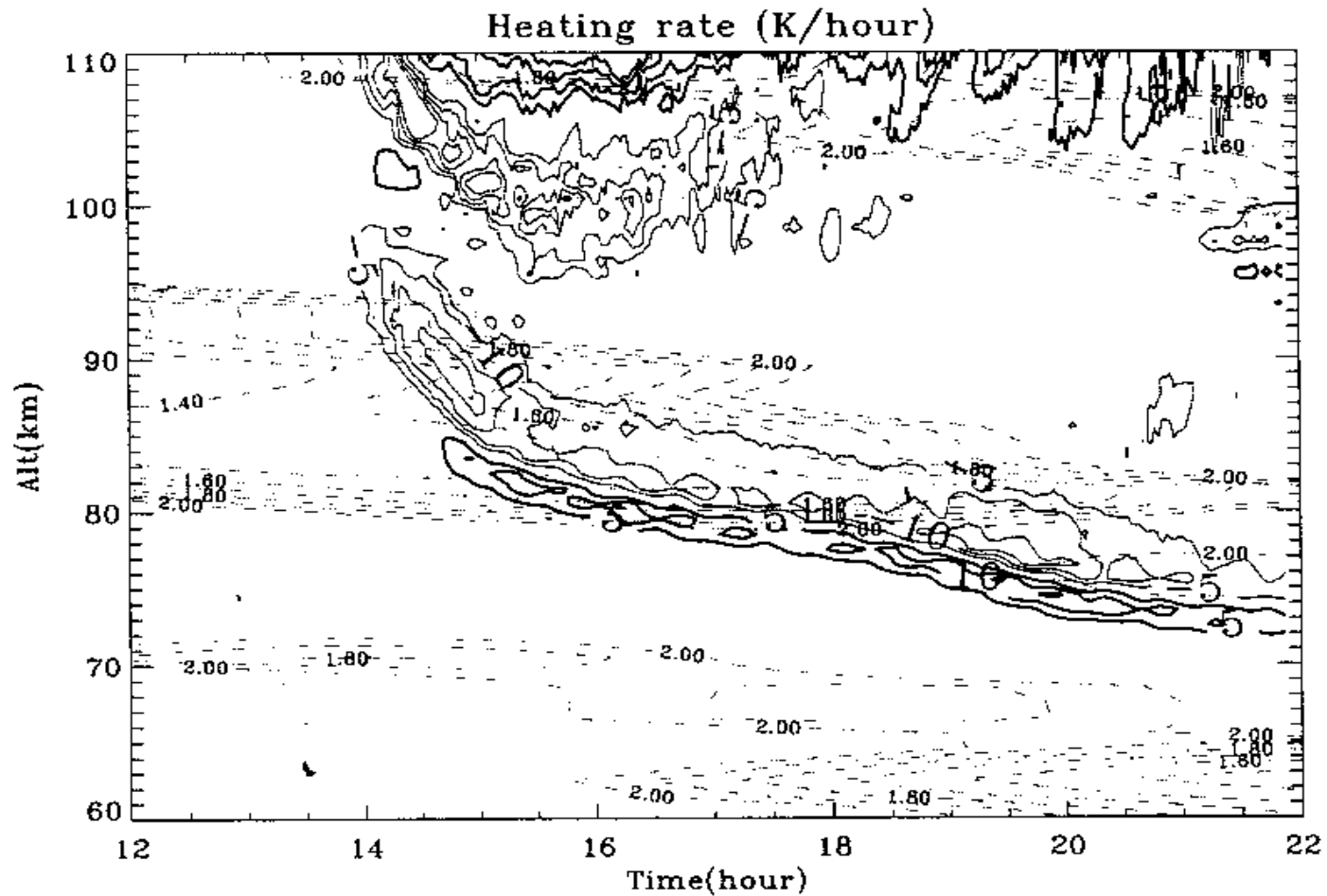
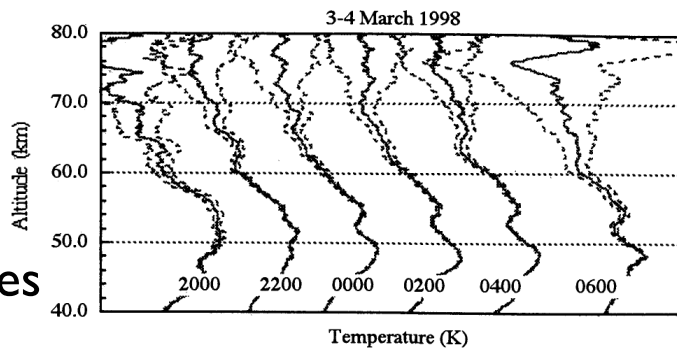


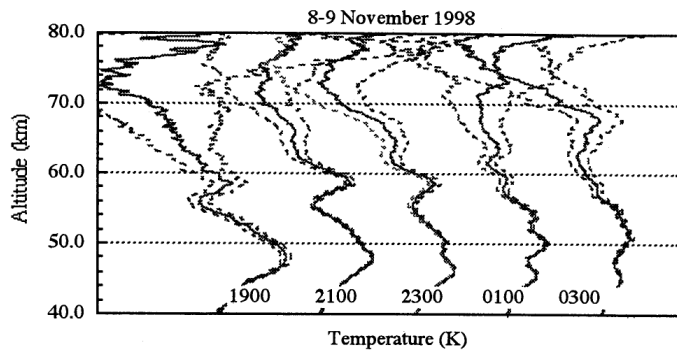
**Figure 4.** Local mean heating rate as a function of time and altitude. The thick solid contour lines are for net heating, and the thin solid curves are for net cooling. The dashed curves are the background state Richardson number on  $\log_{10}$  scale.

Results show combination of heating (bottom side) and cooling (top side)

constant MIL  
at low altitudes



MIL fades



MIL appears

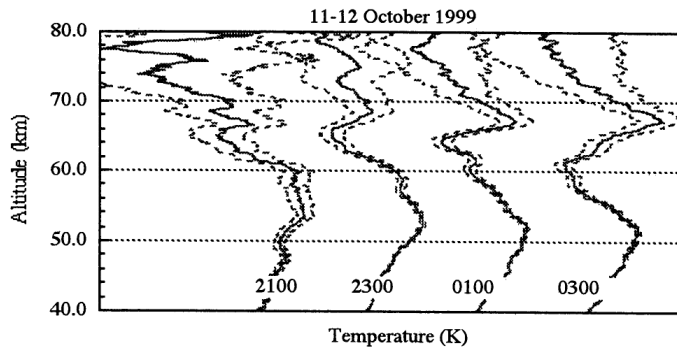


**Figure 1.** Sequence of 2 h temperature profiles measured with the CRL Rayleigh lidar at Poker Flat. The observations represent periods where a mesospheric inversion layer appears relatively constant during the period (top: 3-4 March 1998), disappears during the period (middle: 8-9 November 1998), and appears during the period (bottom: 11-12 October 1999). Time is Local Standard Time (UT - 9 h).

Alaskan observations at Poker Flat by Cutler, Collins show occasional detections of MILs but with different properties than the French MIL events.

Results interpreted as production of MIL through the breaking of a long period GW.

No indication of tidal modulation

# Summary

There are three major sources for the production of MILs.

- Breaking of long period GWs. Happens occasionally.
- Planetary wave activity - when enough GW events to make a zero wind line, absorption of PW takes place to produce a “lower” MIL. Occurs almost all the time during winter at mid-latitudes.
- GW events combined with tidal wave decrease stability and contribute to the formation of a critical layer that causes the GW to break - creates “upper” MIL



# What are the dynamics for the higher MLT altitudes?

Enter the Giant Na UVT lidar instruments:

- Starfire, Albuquerque, NM
- AF AEOS optical facility on Maui, Hawaii

Complex transmitter, big telescope with PMT, high temporal and altitude resolution, excellent accuracy for U,V,T

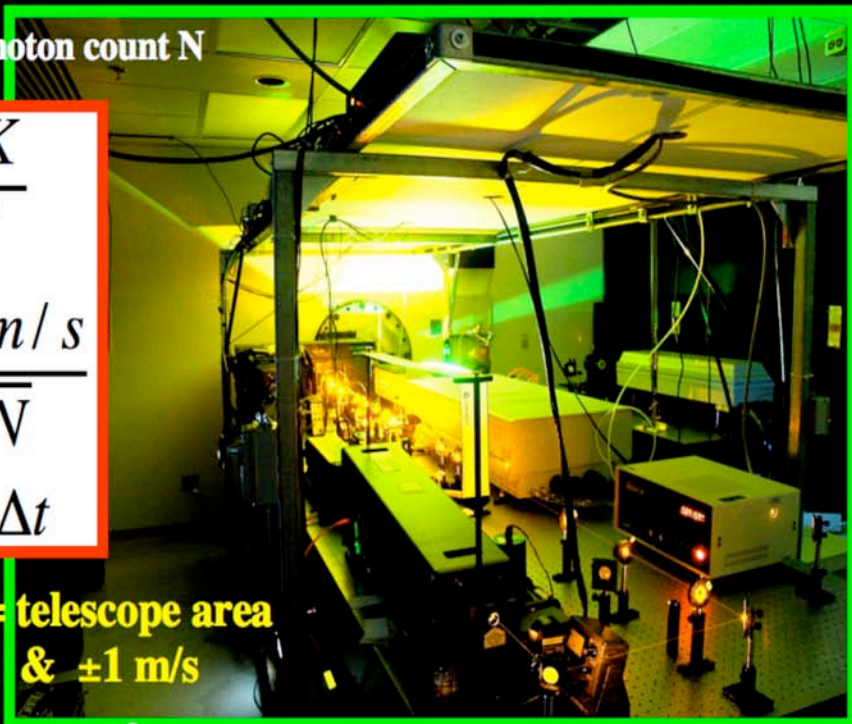
Objective: Measure height variation of stability parameters  $N^2$  and R

Accuracy depends on photon count  $N$

$$\Delta T \approx \frac{250K}{\sqrt{N}}$$
$$\Delta V \approx \frac{200m/s}{\sqrt{N}}$$
$$N \propto PA\Delta z\Delta t$$

**P = laser power**   **A = telescope area**  
 **$N \sim 10^5$  for  $\pm 1 K$  &  $\pm 1 m/s$**

**AEOS =  $10.6 m^2$**





Illinois Na W/T lidar in operation at Starfire Optical Range



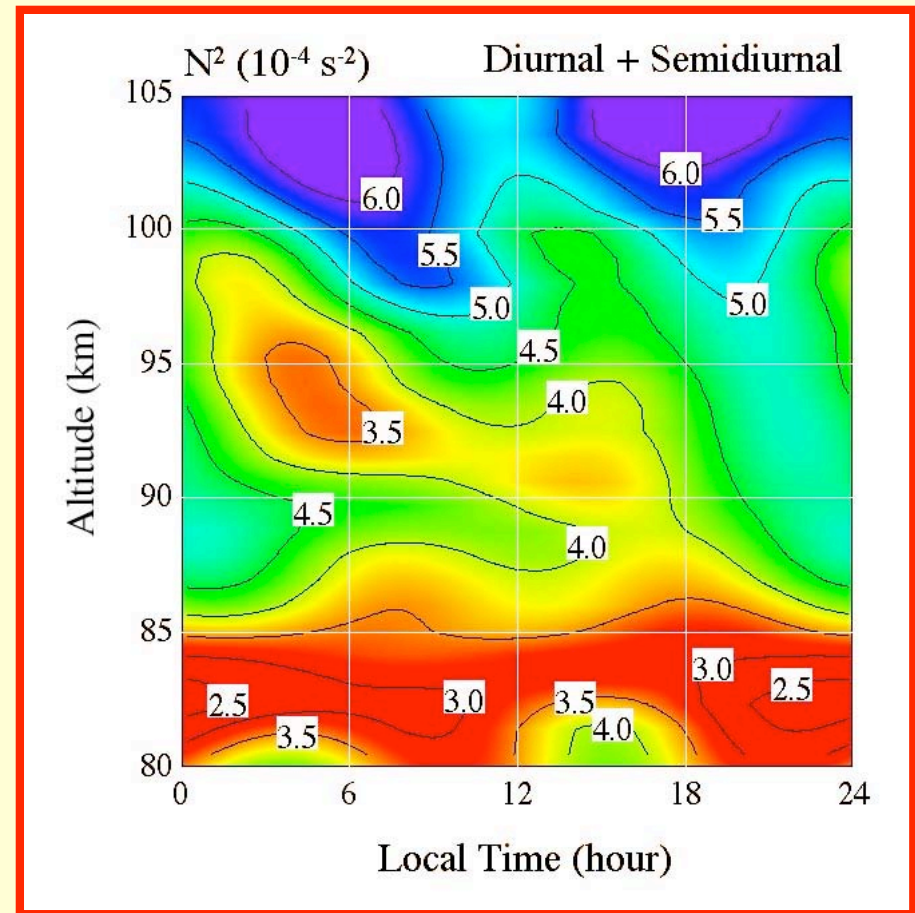
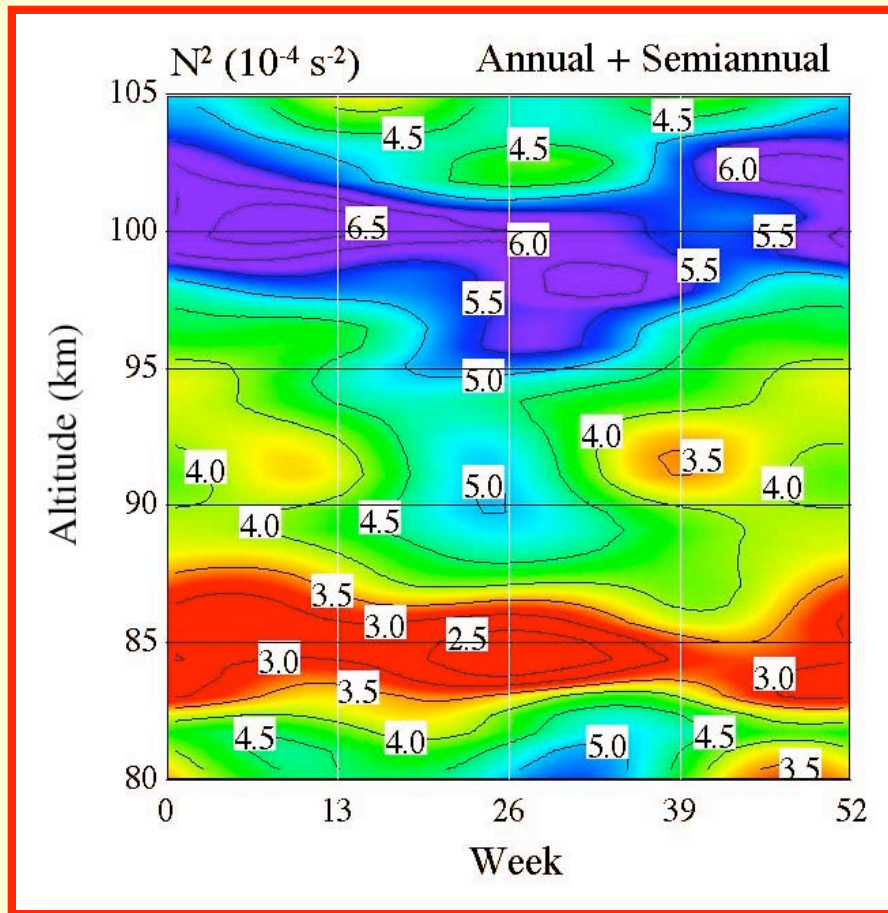
The 3.5 m telescope at Maui

$$N^2 = \frac{g}{T} \left( \frac{\partial T}{\partial z} + \frac{g}{C_p} \right)$$

$$0 < Ri = \frac{N^2}{(\partial u / \partial z)^2 + (\partial v / \partial z)^2} < \frac{1}{4}$$

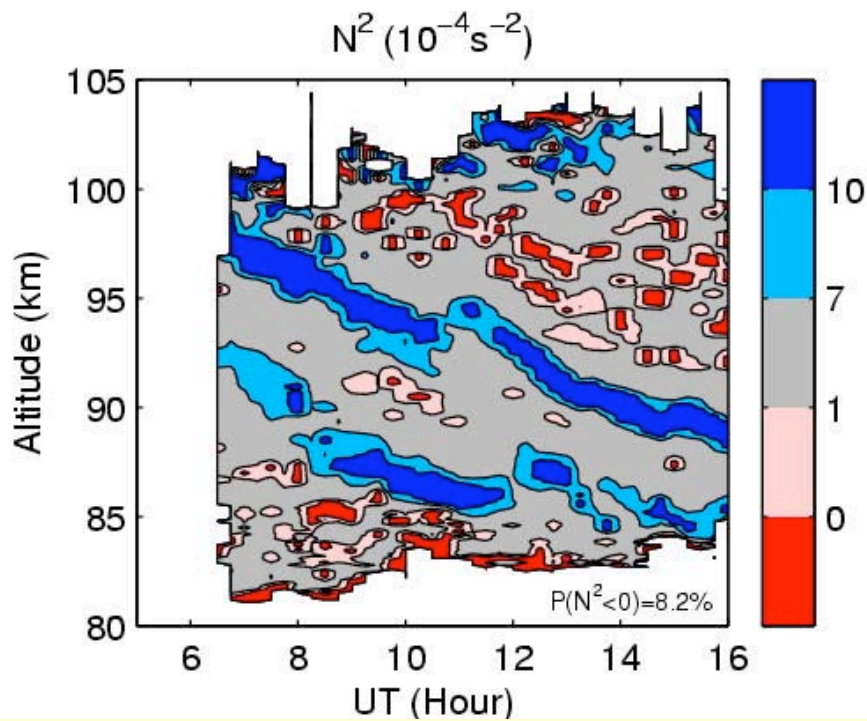
The giant lidar telescope aperture combined with the Na lidar capability to measure U, V, and T allows determination of atmospheric stability with excellent height and time resolution.

# Mean Stability Structure of Mesopause Region

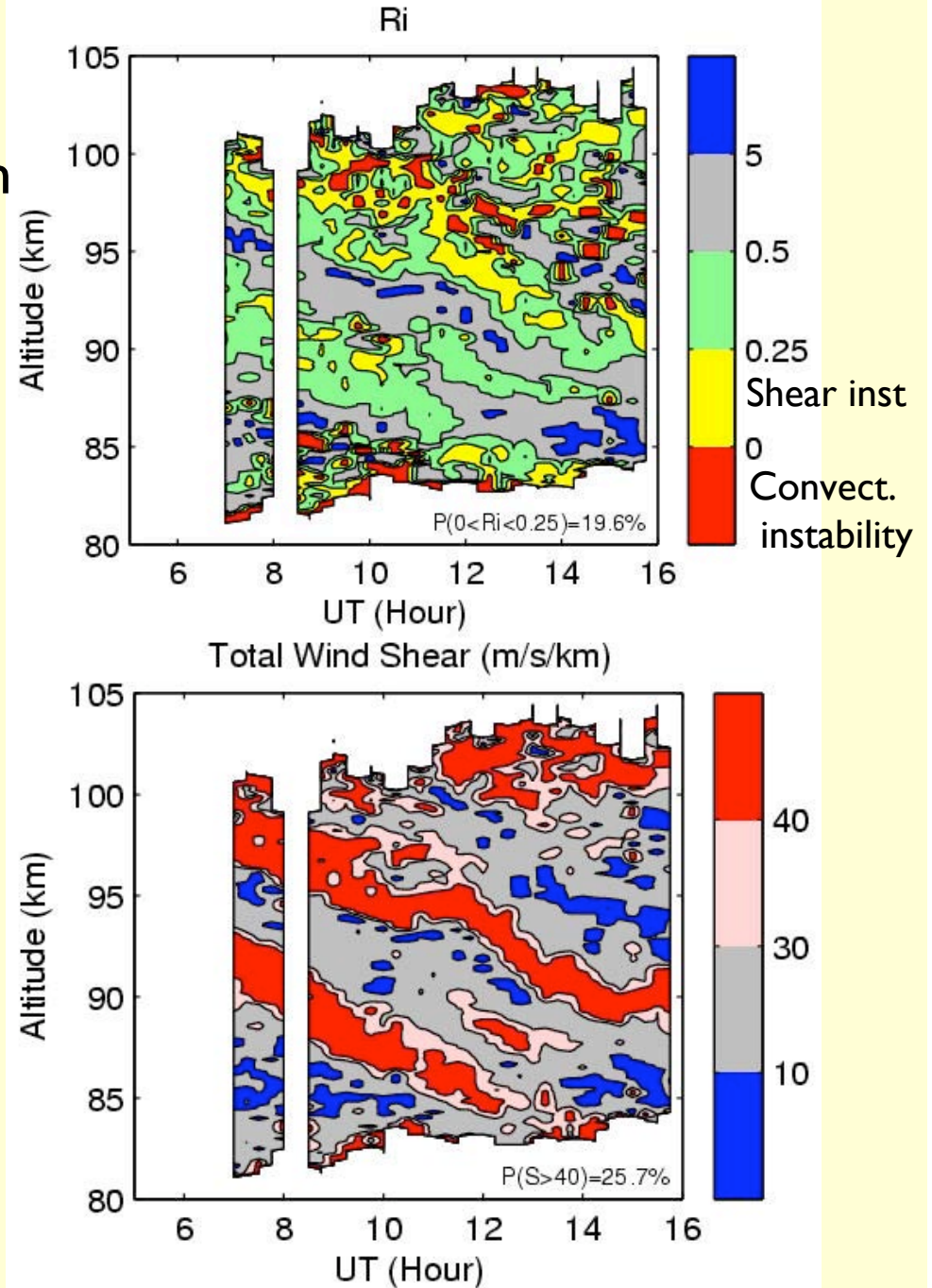


Averaged U, V, and T results show that the atmosphere is generally least stable ( $N^2$  smallest) near 85 km and most stable ( $N^2$  largest) near 100 km

Measurements from Starfire show instability regions with high shear exhibiting a tidal phase progression



Shear region slightly higher in  $h$  relative to stability region



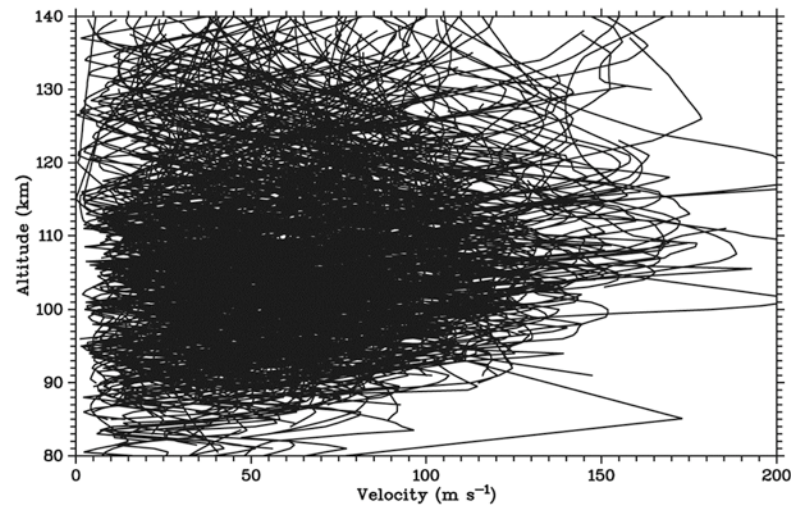


**Figure 2.** Superposition of the wind speed profiles for all the midlatitude and low-latitude chemical release wind profile data.

From Larsen, 2002

Chemical release winds from 4 decades of observations at low latitude sites.

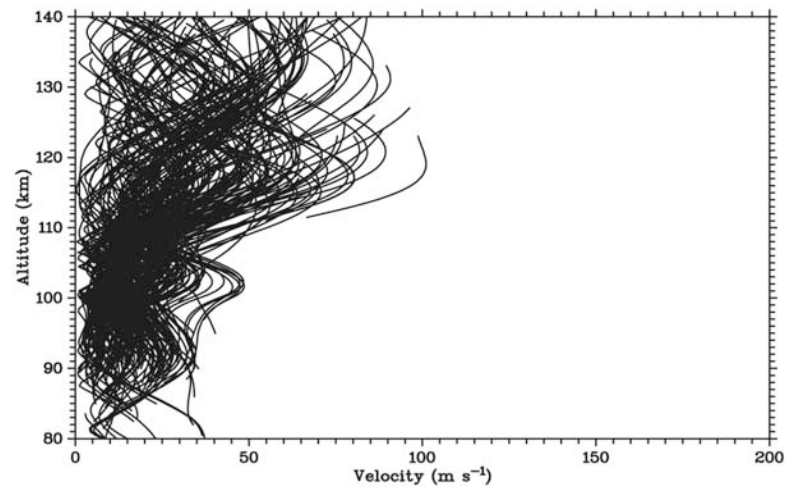


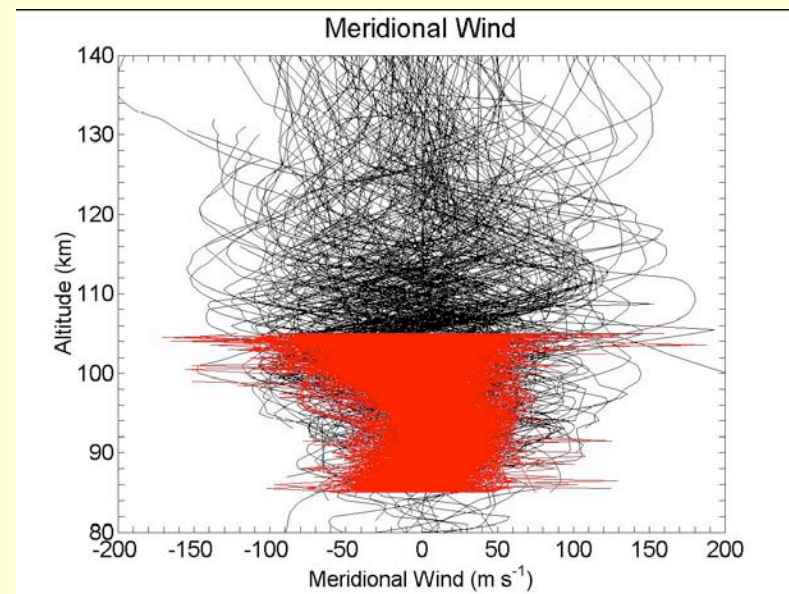
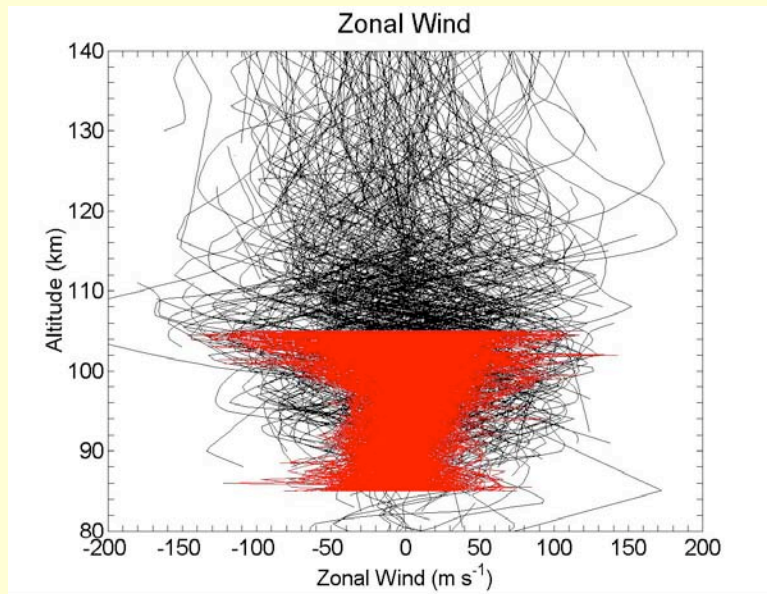
**Figure 14.** Superposition of the wind speed profiles calculated with the Horizontal Wind Model (HWM) for the times, locations, and magnetic activity conditions corresponding to each of the profiles in the chemical release data set.

HWM model predictions for same times and places

MLT winds are generally in excess of  $50 \text{ ms}^{-1}$  above 90 km  
 Much larger than HWM predictions.

## Distribution of winds for latitudes equatorward of $60^\circ$ from four decades of chemical release wind measurements

---

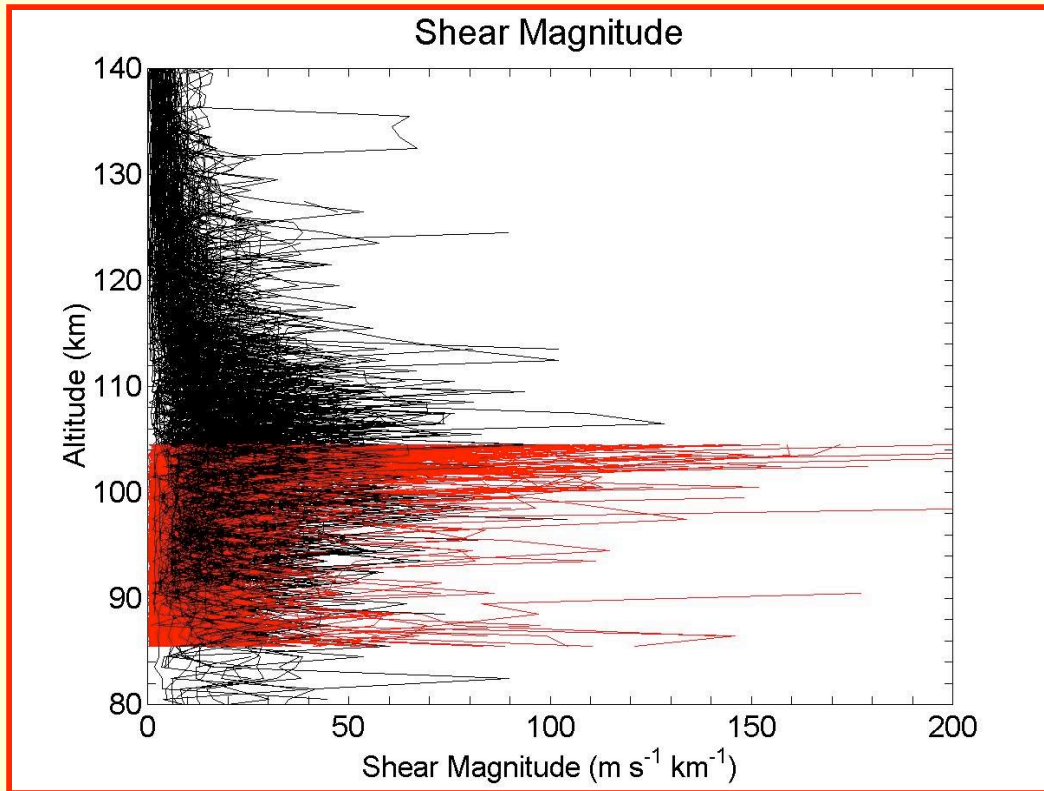


...compared with several years of lidar wind measurements from New Mexico and Hawaii (Zhou et al., 2006)

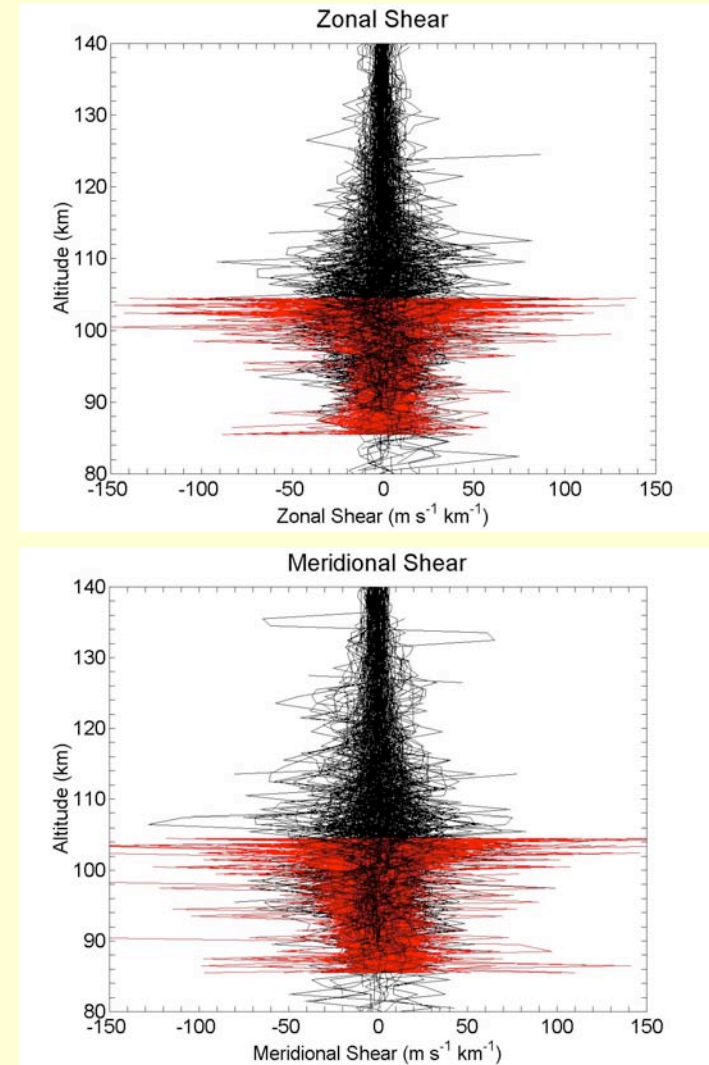
Excellent agreement between the two different sets of results



# Shear profiles determined for chemical release and lidar data



Mesosphere altitudes of 100-105 km are characterized by high values of shear



## STARFIRE Na U/TMA Wind Comparison

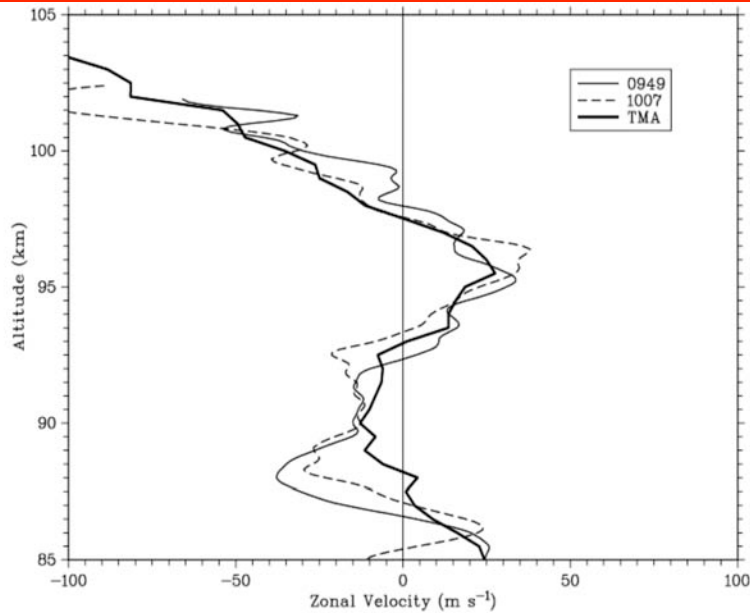


**Figure 2.** Comparison of the zonal wind component derived from the upleg TMA trail with the zonal wind component derived from the lidar radial Doppler velocity measurements in beams 1 and 2. The heavy line is the chemical tracer wind profile. The two lighter lines show the lidar winds for periods of ten minutes before and after the rocket launch.

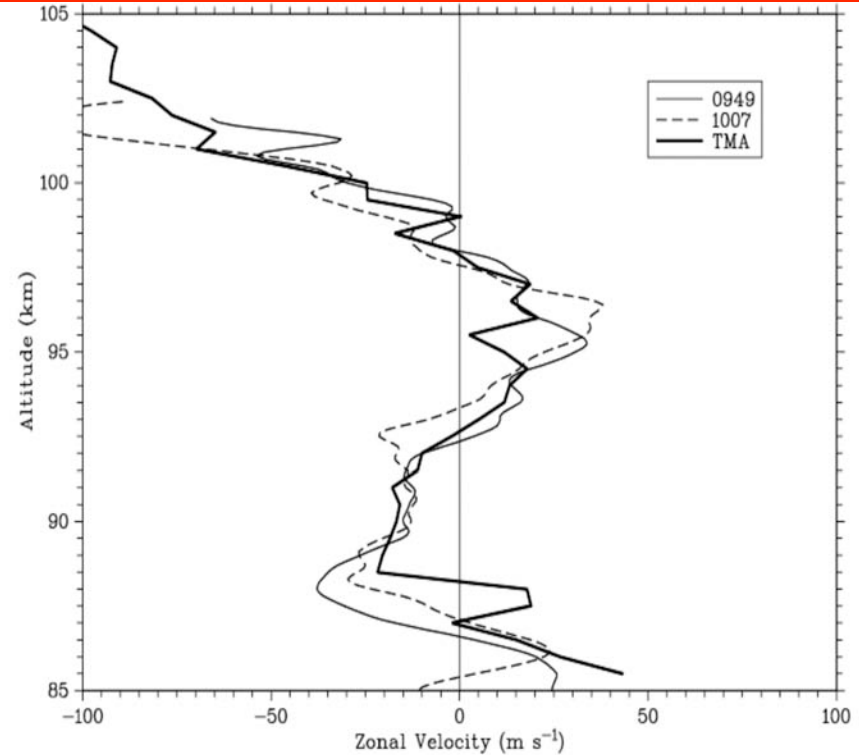
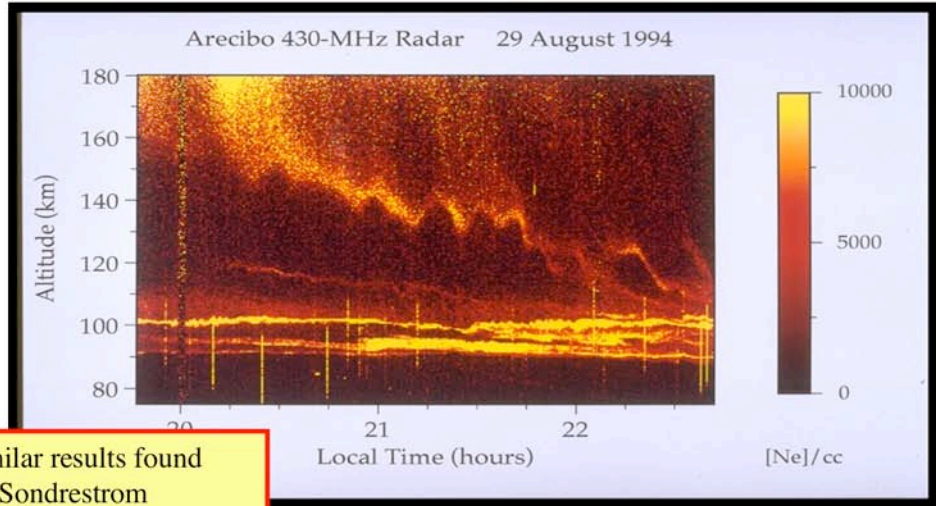


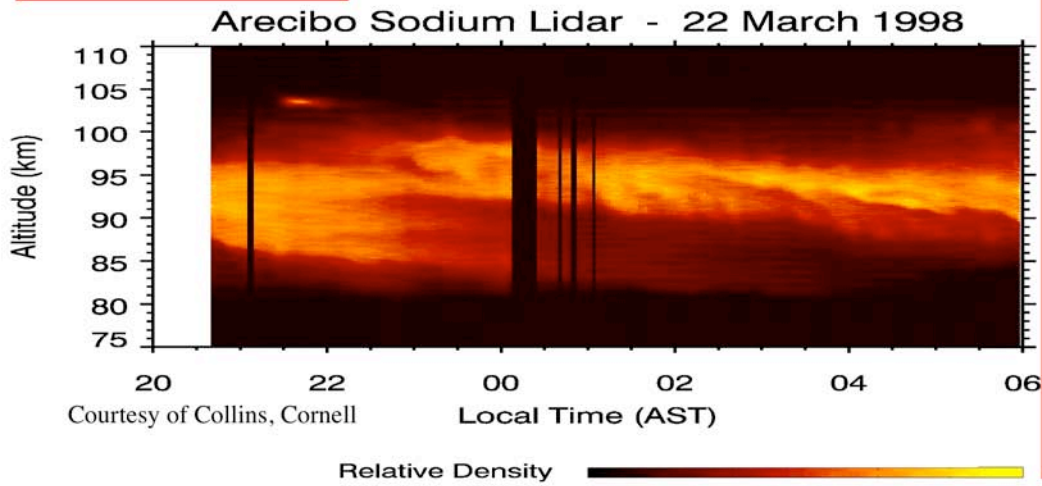
**Figure 4.** Comparison of the zonal wind component from the downleg TMA trail with the zonal wind from the lidar.

TMA winds are in excellent agreement with Starfire Na winds



Similar results found for Sondrestrom (Heinselman et al., 1999)

The structure of the MLT region is rich and complex with a high degree of variability. Unexpectedly, in the COQUI II campaign, examples such as these were observed routinely over many nights (~30). CEDAR phase III needs to have a portable temperature and wind capability in the MLT region to make possible campaigns designed to study the neutral dynamics that underlies the variability of the development of these intermediate and sporadic layers.



Courtesy of Collins, Cornell

Interesting results can be seen in Na density lidar observations, especially when compared with Arecibo ISR observations of sporadic layers

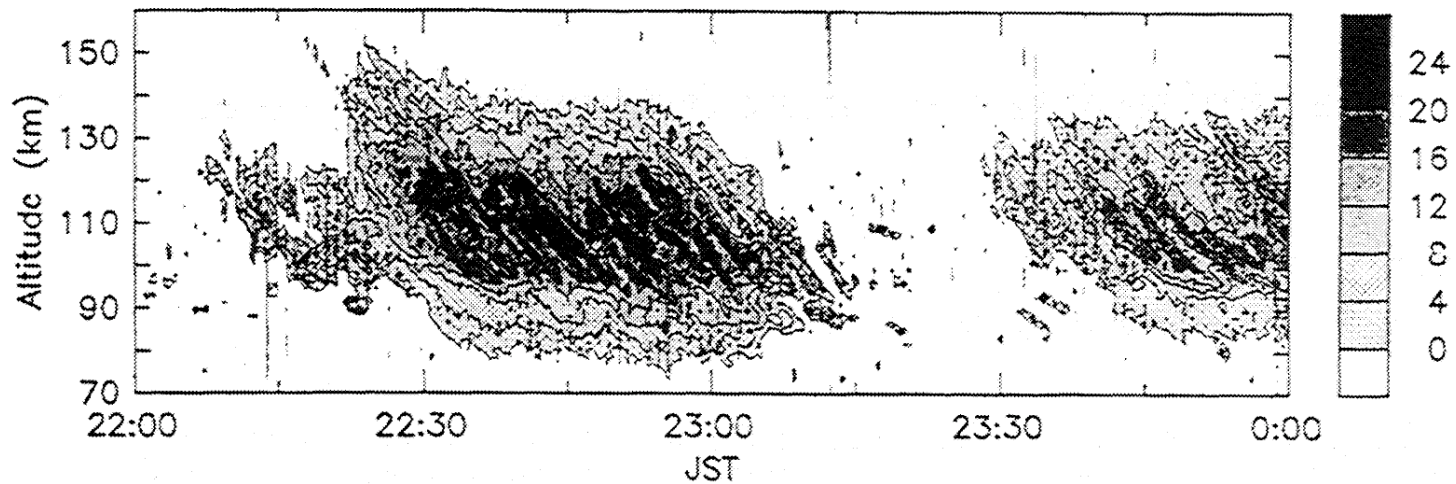


**Figure 1.** An example of the quasiperiodic echoes observed with a HF radar that was located at Tanegashima in southern Japan. JST, Japan Standard Time.

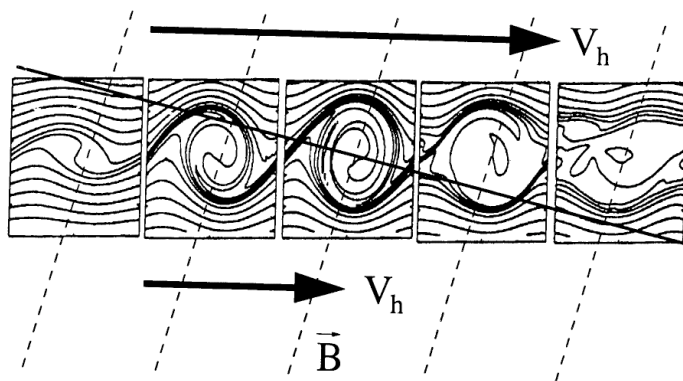


**Figure 6.** Diagram showing the basic mechanism in which vertical displacements of the ionization are induced by Kelvin-Helmholtz billows generated by an unstable neutral shear. The heavy arrows show the neutral flow above and below the layer. The light dashed lines are the magnetic field lines. The heavy solid line shows a radar ray path through the structure.

An interesting radar phenomenon called “QP echoes” is shown in this example observed by a Japanese HF radar.

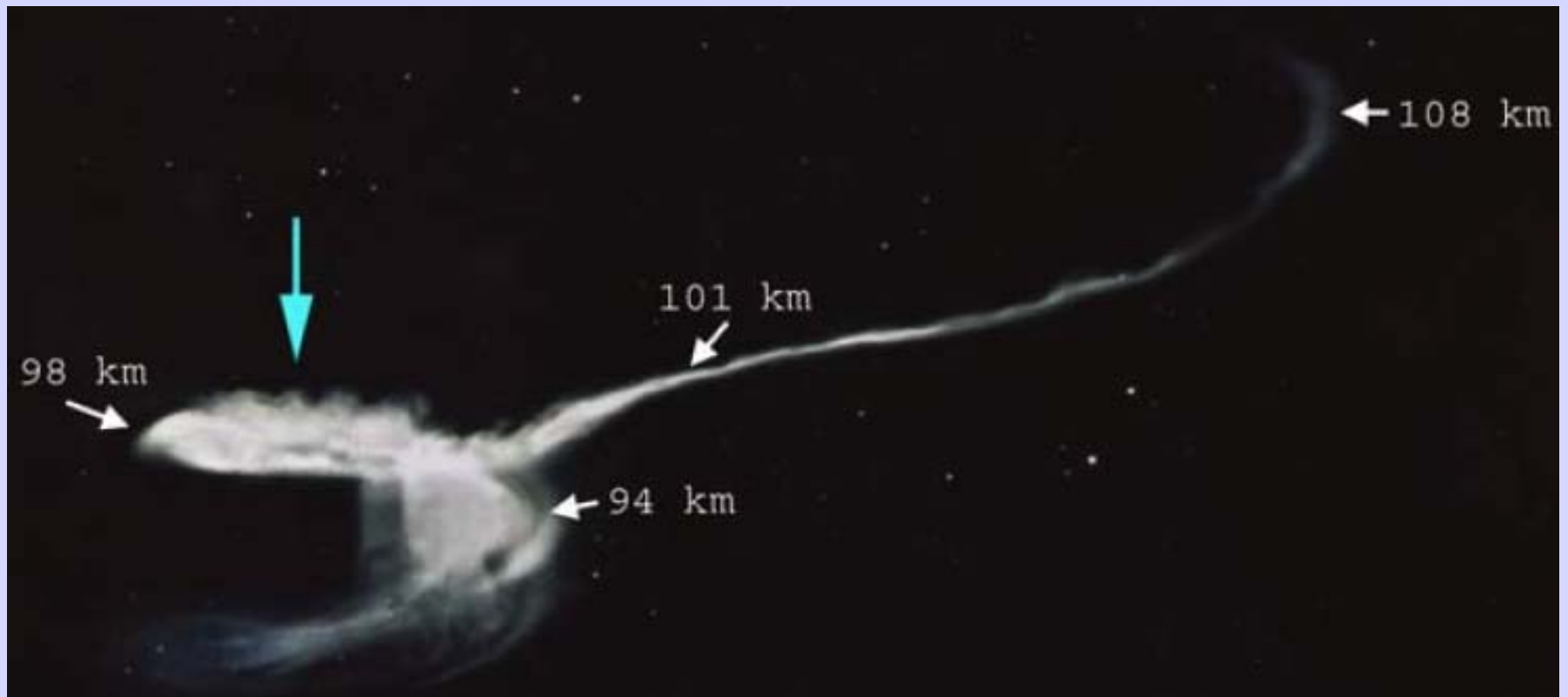
Larsen [2000] suggested that the source of these echoes is the back-scattering from scattering centers within KH billows that are characteristic of unstable shear layers in the MLT region.

These “curls” look familiar:



Common features in the  
atmosphere boundary layer





A photograph of the TMA TOMEX trail on the downleg. The arrow points to the KH billows which occurs between 96 and 99 km. Starfire lidar observations indicate layer of dynamical/convective instability near vicinity of the billows.

Hecht et al.[2004]

**Image of upleg portion of SEEK 2 trail  
viewed from Kochi, Japan**



(Larsen et al., Ann. Geophys., 2005)

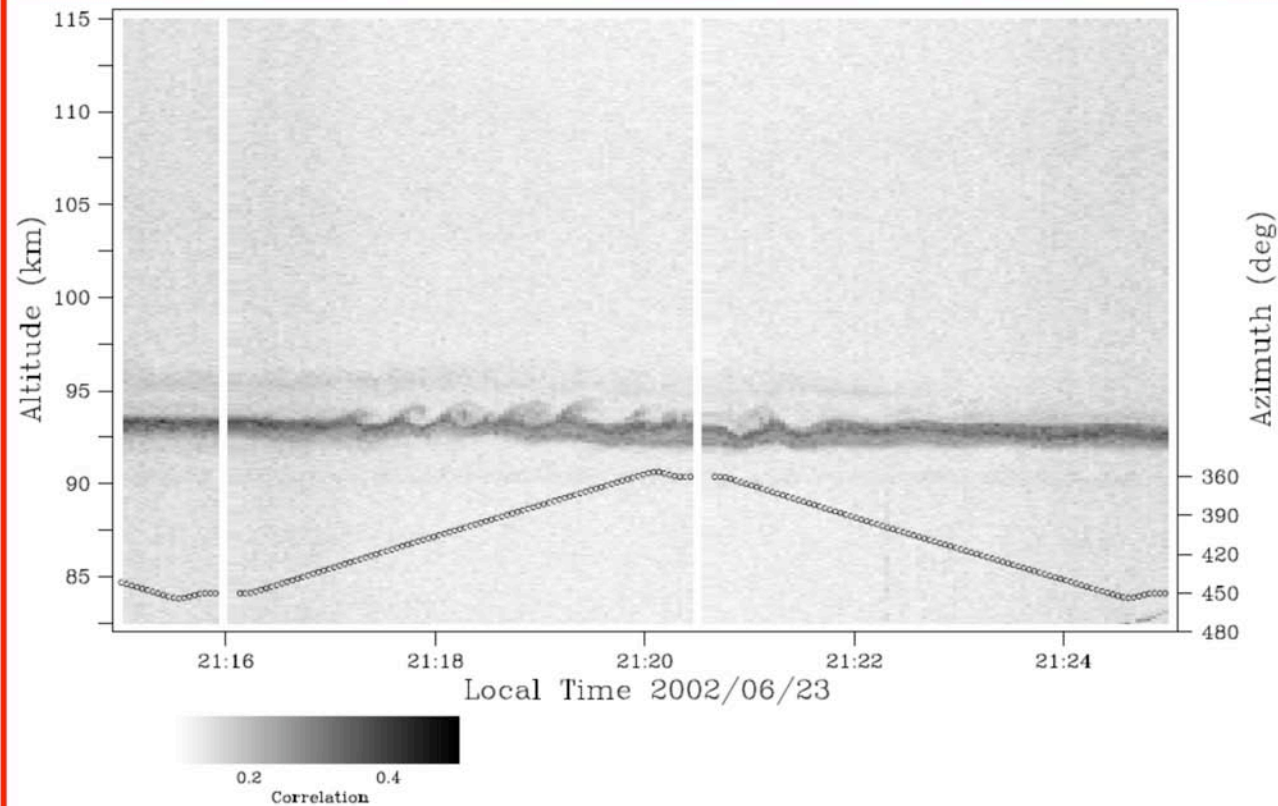
Structure is reminiscent of KH billows and appears in the altitude range between 102 and 108 km in the upleg portion of the trail.

Horizontal wavelength approx. 5 km

Vertical wavelength approx. 2 km

## Hysell, AGU spring 2007

### *Arecibo coded pulse*

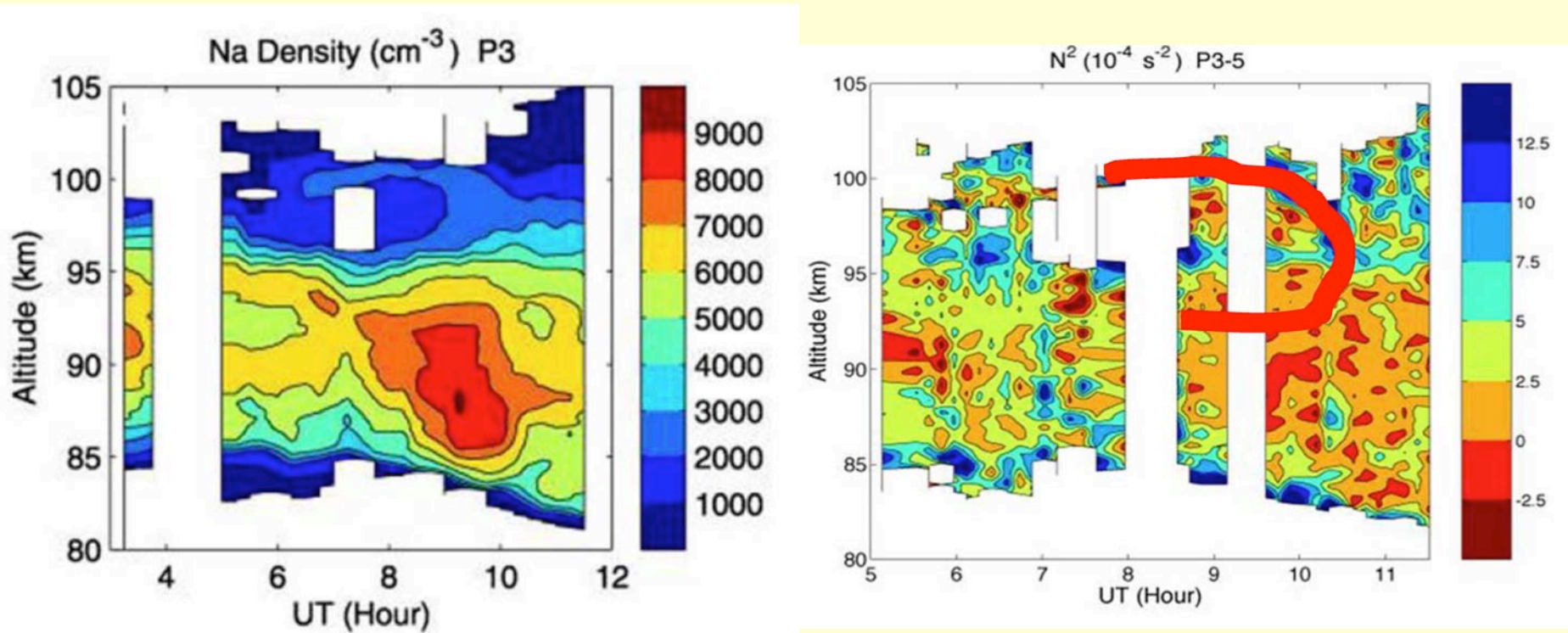


Arecibo 430 MHz radar measurements obtained by Hysell and Larsen show what looks to be KH curl structure at 93 km.

It can be concluded that KH curl structure is a common feature of the mesosphere dynamics and plays an important role in mixing the air.



# Vortex rolls



An interesting feature seen in Na densities - “convective roll”.

is associated with low stability at base of curl and high stability at top, i.e., with the inflection point of the shear

## Further examples “reverse” rolls are also seen

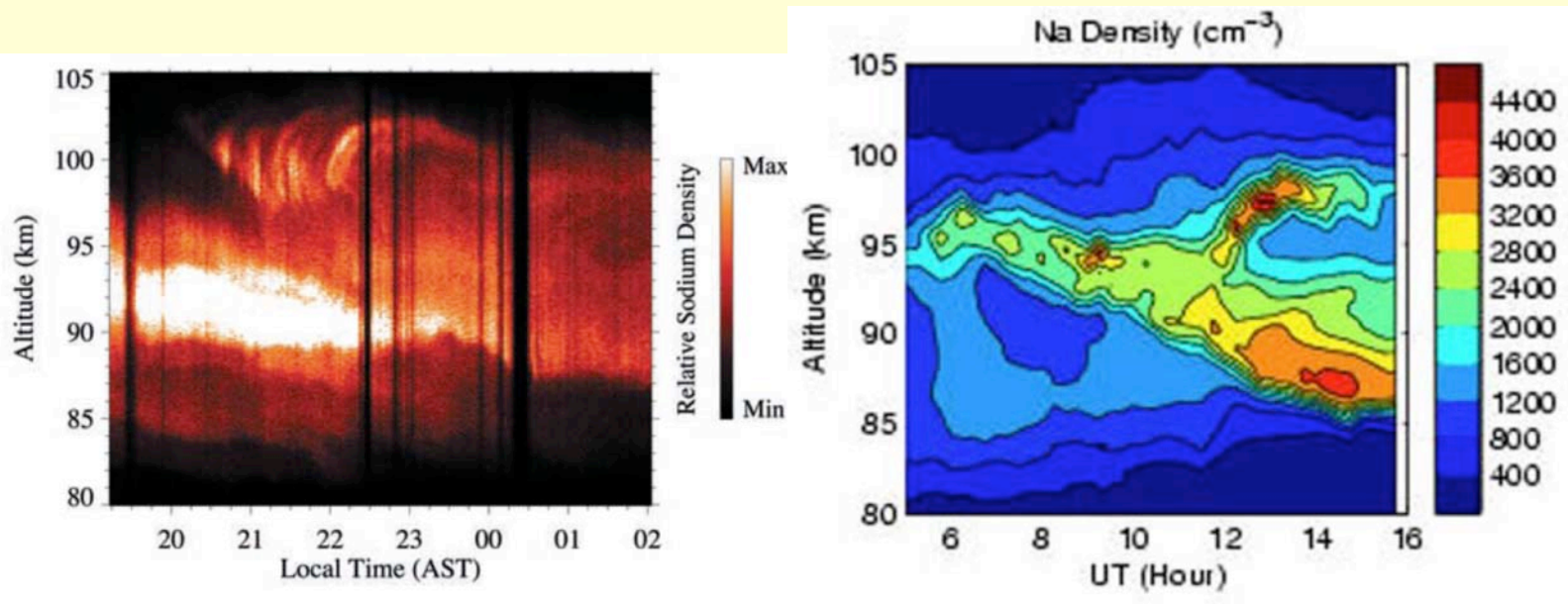


Figure 7. Sodium lidar density measurements from al.[2003]  
Arecibo, Puerto Rico, on 9 February 1999.

These “roll” structures tend to be mesoscale in dimension  
implying organized behavior over periods of 3 hrs. and heights ~5-6 km

## What is the importance of these vortex turbulent structures?

In the style of Tim Russert, from Larsen et al. [2004]

“ [23] Finally, the vortex rolls in the boundary layer often generate a high-speed flow near the top of the rolls. The nocturnal jet, as it is known, is due, at least in part, to the decoupling that results when the flow moves from the highly mixed region associated with the low-stability layer to the less well-mixed region in the high-stability capping layer.”

The question here is why are MLT winds so large?

Could not the same physical process that produces the nocturnal jet also generate the high winds characteristic of the MLT region?

GUVI and Fe lidar evidence indicate that prevailing winds at MLT altitudes (100-120 km) are indeed large.

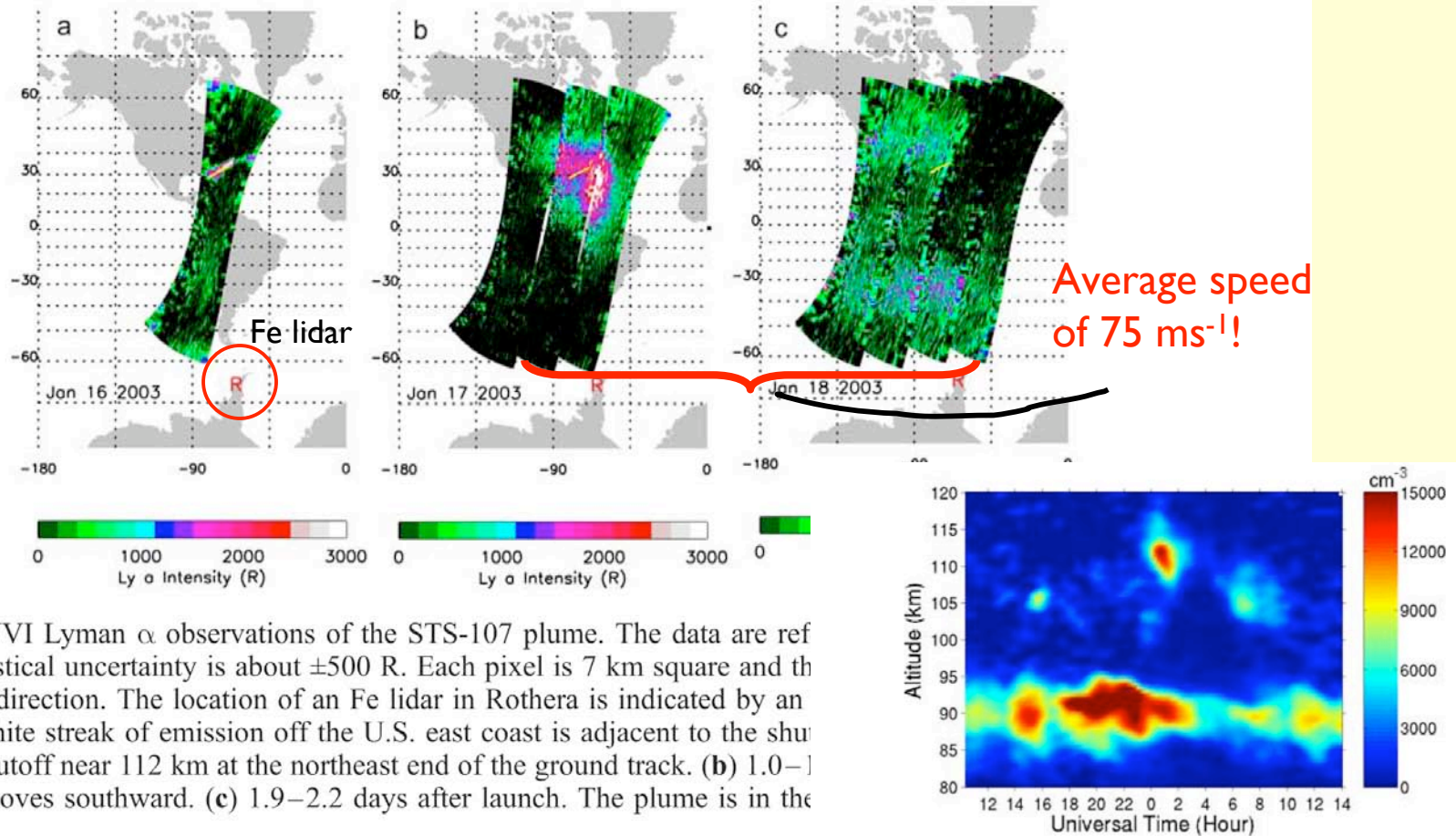


**Figure 1.** GUVI Lyman  $\alpha$  observations of the STS-107 plume. The data are ref where the statistical uncertainty is about  $\pm 500$  R. Each pixel is 7 km square and th pixels in each direction. The location of an Fe lidar in Rothera is indicated by an launch. The white streak of emission off the U.S. east coast is adjacent to the shu engines were cutoff near 112 km at the northeast end of the ground track. (b) 1.0–] the effluents moves southward. (c) 1.9–2.2 days after launch. The plume is in the

**Figure 2.** Fe densities over Rothera, Antarctica: 19–20 January, 2003. The observations, made 2.8–4.0 days after launch of STS-107, have a vertical resolution of  $\sim 1$  km and a temporal resolution of  $\sim 1$  hour. The maximum near 112 km is  $1.5 \times 10^4 \text{ cm}^{-3}$  ( $\pm 200\text{--}300 \text{ cm}^{-3}$ ). There is no known natural source of neutral Fe above 100 km.

Shuttle burn releases exhaust Fe contaminant that is detected in the Antarctica with the iron Fe Boltzmann lidar indicating average speed was in excess of  $44 \text{ ms}^{-1}$ .

## Summary re mesosphere instabilities

- The MLT region of  $\sim 100$  km includes layers of high shear, low stability (perhaps even unstable) and are populated with interesting dynamical features such as KH billows (local scale) and convective roll structures (mesoscale). The shear layer would not have been detected without the Na lidar measurements of U,V,T profiles with excellent spatial and temporal resolution
- Mesospheric winds near  $\sim 100$  km are generally quite large, possibly in excess of what tidal waves (migrating, non-migrating) might generate - **why?**
- New dynamical structures previously not appreciated have been detected: KH billows, convective rolls. What other species in the dynamical zoo might there be?
- The study of mesospheric dynamics might be called the boundary layer meteorology of MLT space physics.

# Closing comments

- MIL structure reasonably well understood as a result of the interaction of a wave, whether GW, PW, or TW, with the medium decreasing the stability of the region, increasing shear, and producing turbulence instabilities. Critical layer interaction significant player in case of GW events.
- Multi-instrument campaigns really a great way of doing mesospheric science: AIDA, ALOHA, TOMEX, Coqui Dos - bring together multiple instruments to measure significant parameters simultaneously: more should be done!
- Hence, wonderful news that a portable Na UVT facility will be funded enabling campaign type of activity so that such structures can be studied in regions of interest: equator, mid-latitudes, polar.
- Recommend strongly development of Rayleigh Doppler lidar capability so to assess the wave filtering taking place below the MLT region and to study more directly the coupling of mesospheric dynamics with that of the stratosphere.